Polymer Chemistry

Cite this: *Polym. Chem.*, 2011, **2**, 2707

www.rsc.org/polymers

REVIEW

Conjugated polymer nanostructures for organic solar cell applications

Jiun-Tai Chen* and Chain-Shu Hsu*

Received 16th June 2011, Accepted 17th July 2011
DOI: 10.1039/c1py00275a

Recently, there has been tremendous progress in the development of polymer-based organic solar cells. Polymer-based solar cells have attracted a great deal of attention because they have the potential to be efficient, inexpensive, and solution processable. New materials, nanostructures, device designs, and processing methods have been developed to achieve high device efficiencies. This review focuses on the fabrication techniques of conjugated polymer nanostructures and their applications for organic solar cells. We will first introduce the fundamental knowledge of organic solar cells and emphasize the importance of nanostructures. Then we will discuss different strategies for fabricating conjugated polymer nanostructures, including topics such as polymer nanowires, nanoparticles, block copolymers, layer-by-layer deposition, nanoimprint lithography, template methods, nanoelectrodes, and porous inorganic materials. The effects of the nanostructures on the device performance will also be presented. Efficiencies higher than 10% are expected for polymer-based solar cells by using new materials and techniques.

Department of Applied Chemistry, National Chiao Tung University, 1001 Ta Hsueh Road, Hsin-Chu, 30049, Taiwan. E-mail: jtchen@mail.nctu.edu.tw; cshsu@mail.nctu.edu.tw; Fax: +886-3513-1523; Tel: +886-3513-1523

Jiun-Tai Chen

Jiun-Tai Chen received his B.S. degree in 1999 and M.S. degree in 2001 from the Department of Applied Chemistry at National Chiao Tung University. He joined Prof. Thomas Russell's group in 2003 and completed his Ph.D. in 2008 at the University of Massachusetts, Amherst in Polymer Science and Engineering, where his thesis work focused on template-based nanomaterials. He then joined the Center for Nano- and Molecular Science and Technology at the University of Texas at Austin with Prof. Paul F. Barbara as a postdoctoral fellow, where he worked on electrogenerated chemiluminescence of conjugated polymers. In the summer of 2010, he joined the Department of Applied Chemistry at National Chiao Tung University as an assistant professor. His research interests include the fabrication and characterization of polymer nanomaterials for optoelectronic applications.

Chain-Shu Hsu

Chain-Shu Hsu received his Ph.D. degree from Case Western Reserve University in 1987 and conducted post-doctoral work at the National Tsing Hua University in Taiwan. He joined the Department of Applied Chemistry of the National Chiao Tung University, Taiwan in 1988 as an associate professor and was promoted to full professor in 1991. Currently he is serving as a vice president and chair professor of the National Chiao Tung University. His research interests include liquid crystalline polymers and conjugated polymers, polymer light-emitting diodes, and organic solar cells. He has published more than 200 research papers and 20 patents. He is currently on the international advisory board of Polymer and editorial boards of the Journal of Polymer Science, Polymer Chemistry, and the Journal of Polymer Research. He received the Excellent Research Award of the National Science Council, Taiwan, in 1994, the Franco-Taiwan Scientific Award for nanomaterials in 2006, Teco and Hou Chin Tui Awards in 2007, and an Academic Award of the Ministry of Education, Taiwan, in 2008.

1 Introduction

1.1 Organic solar cells

In recent years, energy-related issues have received considerable attention concerning the rising costs of fossils and growing global greenhouse gas.[1] There is an urgent need to develop clean and renewable energy technologies. The largest potential source of renewable energy is the solar energy incident on the Earth's surface.[2] Solar cells are devices which convert solar energy directly into electricity, and the most common material used for solar cells is silicon.[3] Although silicon-based solar cells exhibit some of the highest power conversion efficiencies, they remain expensive because of the intensive processing techniques and the high cost of purified silicon.[4] In this context, organic molecules are alternative candidates for solar cells because of their low cost and high processability.[5,6]

The most widely studied organic solar cells are polymer-based solar cells using conjugated polymers. Most conjugated polymers have high absorption coefficient and high percentage of absorbed photons that can produce an excited state (>90%).[7] There are other advantages for using the polymer-based organic solar cells. First, the photo and electronic properties of the conjugated polymers can be fine-tuned by changing the chemical structures through advances in organic chemistry.[8,9] Second, simple coating or printing processes can be used which will reduce the cost of the fabrication process.[10] Third, the mechanical flexibility allows the development of flexible devices.[11] In addition to organic solar cells, conjugated polymers have been used in other types of optoelectronic devices such as organic field-effect transistors (OFETs) or organic light-emitting diodes (OLEDs).[12,13]

Although significant progress has been made in polymer-based solar cells, the maximum power conversion efficiencies (PCEs) are still not sufficient to be marketable. Also, the commercialization of the polymer-based solar cells is limited by the lifetimes of the devices which are affected by the water and oxygen in the atmosphere. Therefore, more research effort will need to be devoted towards the commercialization of polymer-based solar cells.[14]

1.2 Working principles of organic solar cells

The typical structure of an organic solar cell is shown in Fig. 1. A hole transport layer, poly(3,4-ethylenedioxythiophene):poly (styrenesulfonate) (PEDOT:PSS), is spin-coated on top of the anode. The active layer comprising the donor and the acceptor is sandwiched between the cathode and the hole transport layer. The process for organic solar cells to convert sunlight into electricity is described as follows: The light-absorbing material with a bandgap in the visible region absorbs photons that excite the electrons from the ground state to the excited state, and bound electron-hole pairs (excitons) are created. The excitons diffuse to the donor–acceptor interface where excitons dissociate into free charge carriers after overcoming the binding energies. The free charge carriers transport to the respective electrodes under the internal electric fields, resulting in the generation of photocurrent.

Power conversion efficiency (PCE) is used to evaluate the performance of polymer solar cells.[5] The PCE of an organic solar cell is determined by the following equation:

$$\mathrm{PCE} = (\mathrm{FF} \times J_{sc} \times V_{oc})/P_{in} \quad (1)$$

where PCE is the power conversion efficiency, FF is the fill factor, V_{oc} is the open-circuit voltage, J_{sc} is the short-circuit current, and P_{in} is the power density of the incident light. The solar cells are usually tested under Air Mass (AM) 1.5G conditions, 100 mW cm^{-2}. These conditions are experienced when the sun is at an angle of about 48° and are considered to best represent the Sun's spectrum on the Earth's surface.[15] Fill factor is the ratio of the actual power limit to the theoretical power limit of a solar cell, which can be calculated from the division of the largest power output (P_{max}) by the product of J_{sc} and V_{oc}, as shown in Fig. 2. Open-circuit voltage (V_{oc}) is the maximum possible voltage across a solar cell. The value of V_{oc} is close to the energy difference between the highest occupied molecular orbital (HOMO) of the electron donor and the lowest unoccupied molecular orbital (LUMO) of the electron acceptor (see Fig. 3).[16] The short-circuit current (J_{sc}) is the current through the solar cell when the voltage across the solar cell is zero.

One of the most promising candidates for polymer organic solar cells is a blend of regioregular poly(3-hexylthiophene) (rr-P3HT) and [6,6]-phenyl-C_{61}-butyric acid methyl ester (PCBM) (Fig. 4).[17] Although the bandgap is only 2.0 eV, P3HT possesses high hole mobility (up to 0.1 $cm^2V^{-1}s^{-1}$) and great self-organization capability.[18,19] The mobility of P3HT is highly dependent

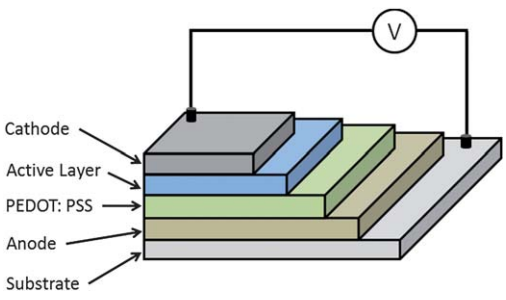

Fig. 1 Typical structure of an organic solar cell. PEDOT:PSS is spin-coated on top of the anode as a hole transport layer. The active layer is sandwiched between the cathode and the hole transport layer.

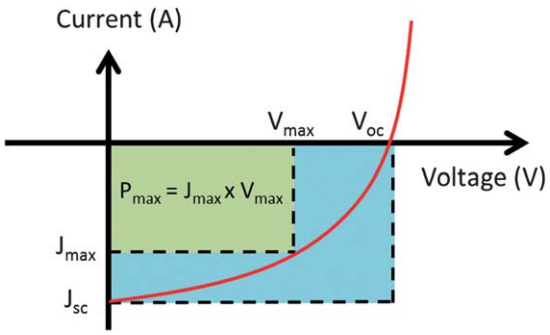

Fig. 2 Current–voltage (I–V) characteristics of an organic solar cell. V_{oc} is the open-circuit voltage and J_{sc} is the short-circuit current. The points where the product of current and voltage is maximized determine the largest power output (P_{max}). The fill factor (FF) is obtained from the division of P_{max} by the product of J_{sc} and V_{oc}.

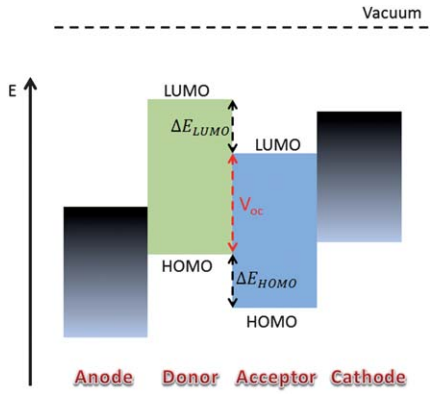

Fig. 3 Energy level diagram of an organic solar cell with a donor–acceptor interface. The open-circuit voltage (V_{oc}) is close to the energy difference between the highest occupied molecular orbital (HOMO) of the donor and the lowest unoccupied molecular orbital (LUMO) of the acceptor.

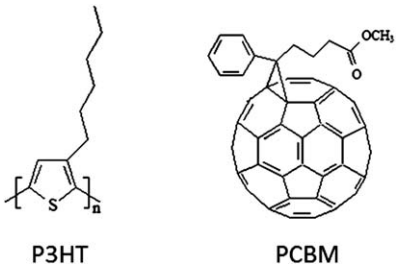

Fig. 4 Chemical structures of poly(3-hexylthiophene) (P3HT) and [6,6]-phenyl-C_{61}-butyric acid methyl ester (PCBM).

on the crystallinity, the orientation of the polymer chains, and the molecular weight. PCBM has a high electron mobility and is soluble in common organic solvents. The combination of P3HT and PCBM dominates the current research in polymer solar cells. They also serve as good model materials to examine different effects on the device performance. In this review, many examples of solar cells based on conjugated polymer nanostructures are related to the fabrication of P3HT nanostructures followed by the deposition of PCBM. For example, P3HT nanorods can be made by a nanoporous template and function as the donor materials. Then PCBM can be deposited on the P3HT nanorods to form an ordered heterojunction.

1.3 Strategies to improve the device performance

After introducing the fundamental knowledge of organic solar cells, we will discuss some common strategies to improve the device performance of organic solar cells. As shown in Fig. 5, these strategies involve designing and synthesizing new materials, changing device structures, controlling morphology, and making nanostructures.

Although the Sun provides a vast amount of energy, only a small portion of the incident sunlight is absorbed because of the large bandgap of organic materials. The bandgap of typical conjugated polymers ranges between 2 and 3.5 eV, which limits the possible absorption of solar energy. For a material with

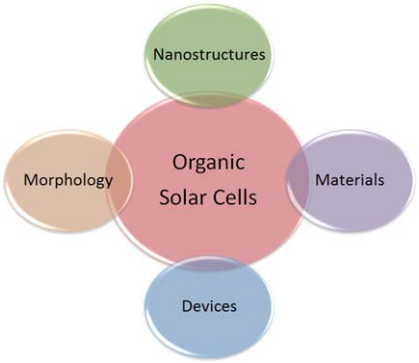

Fig. 5 Main research directions to improve the device performance of organic solar cells including materials, devices, morphology, and nanostructures.

a band gap of 1.1 eV (1100 nm), 77% of the incident solar energy on the Earth's surface can be absorbed.[5] Therefore, it is necessary to design and synthesize new low bandgap conjugated polymers that can absorb more of the solar energy. It also need to be noted that the device performance can be affected by not only the bandgap, but also the position of the HOMO and LUMO levels of the conjugated polymers which can limit the V_{oc} of the device.[16] The absorption spectrum and energy levels of conjugated polymers can be tuned by functionalization. Many synthetic efforts have been made to develop new low bandgap polymers.[20,21]

Towards the commercialization of organic solar cells, several issues with the standard organic solar cells have to be considered. First, the low work-function metal electrodes, such as calcium and lithium, are unstable under ambient conditions.[22] Second, the hole transport material, PEDOT:PSS, has been shown to react with the ITO electrode, resulting in the degradation of the devices.[23] The acidic PEDOT:PSS layer is also detrimental to the active layer. To resolve these issues, inverted device structures have been developed which allows the use of more stable high work-function metals.[24] In the inverted structures, electrons and holes exit the device in opposite directions, comparing with the normal device structures. ITO serves as the cathode and a more stable, high-work-function metal is used as the anode. The stability of the inverted device under ambient conditions is dramatically improved, compared with the normal device.[25]

The morphology control of the active layer in solar cells is of great importance in improving the device efficiencies. Since exciton dissociation occurs at the interface of the donor and acceptor materials, a large interfacial area should allow maximum exciton dissociation.[26] It has been shown that post-treatments such as thermal annealing above the glass transition temperature (T_g) of the active material are crucial for the device performance, although low band-gap polymers often show degraded device performance after thermal annealing.[27,28] By annealing, the active materials such as the P3HT chains can organize and self-assemble into a more regular, crystalline state, resulting in higher charge mobility. Acceptor materials such as PCBM will also diffuse and aggregate to form larger domains. The device performance is improved by the maximized donor–acceptor interfacial area and the higher degree of crystallinity. But the optimized morphology and phase segregation of the

active materials are at intermediate states that will form more equilibrium morphologies upon further annealing.[29] With longer annealing time, the donor–acceptor interfacial area decreases owing to larger size phase separation, resulting in lower efficiencies. Many efforts have been made to maintain the optimized morphology of the donor–acceptor heterojunction. Photocrosslinkable P3HT copolymers or fullerene derivatives, for example, are used to stabilize the bulk heterojuncitons.[30–33] The morphology of the heterojunction can also be preserved by using a block copolymer containing oligothiophene and fullerene side groups as a compatibilizer.[26]

Solar cells based on polymer heterojunction are considered to be better than single component polymer solar cells. The interfacial area between the donor and acceptor materials can be increased and more exciton dissociation can occur to generate higher photocurrent. The concept of heterojunction was first introduced by Tang: bilayer heterojunction structures can be used for creating efficient charge separation.[34] This concept was then applied to polymer-based solar cells and the efficiency was dramatically increased, because of the large donor–acceptor interfaces.[35] Bulk heterojunction polymer solar cells are usually based on two components including an electron-donating material (donor) and an electron-accepting material (acceptor). Disordered structures on the nanoscale will result in poor device efficiencies due to exciton recombination and poor mobility.[36] It is necessary to control the morphology of the active materials on the nanoscale. There are several possible morphologies for the donor–acceptor heterojunction. The simplest case is the bilayer structures, where the electron-donor is first deposited on the anode, followed by the deposition of the electron-acceptor (see Fig. 6a).[37] But the bilayer devices only allow excitons to dissociate near the donor–acceptor interface, resulting in low device efficiencies.[38] In order to improve the solar cell efficiencies, it is critical to control the donor–acceptor interface in order to optimize charge separation and charge migration to the electrodes. The most common way to make bulk heterojunction organic solar cells is by blending donor and acceptor materials. The interfacial area between donor and acceptor significantly increase compared with the double layer devices, resulting in improved device efficiencies (see Fig. 6).

In order to achieve high device performance, the domain sizes of the donor and the acceptor need to be optimized. The optimal domain size is related to the diffusion length of excitons. Exciton diffusion length is the average distances the excitons travel before recombination, which depends on the lifetime and the diffusion coefficient of the excitons. The diffusion length of excitons in the polymer-based organic solar cells is usually around 5–10 nm. Therefore, the ideal size of the nanostructures should be close or equal to the diffusion length. A larger interface is produced by reducing the domain sizes, allowing more exciton dissociation while reducing the recombination of excitons. Fig. 6c represents the ideal heterojunction morphology of organic solar cells, where the donor and the acceptor domains are aligned normal to the electrode surfaces.[39] Also, there should be a continuous donor film in contact with the anode and a continuous acceptor film in contact with the cathode. The thickness of the heterojunction also needs to be optimized. The light absorption depends on not only the bandgap of the materials, but also the thickness of the absorbing materials. The absorption coefficients of conjugated polymers are relatively high ($\sim 10^5$ cm^{-1}), and the film thickness of 100–200 nm should allow efficient absorption.[5,36] Higher thickness will increase chances of recombination of the excitons, even though more photons might be absorbed. The crystallinity and charge mobilities can also be changed by the confinement effect at the nanoscale. For example, the hole mobility in regioregular P3HT was found to enhance by a factor of 20 when the polymers were infiltrated into straight nanopores of an anodic alumina template.[40] In addition to the diffusion length of excitons, the optimized domain sizes also depend on the packing of molecules, which affects the charge transport in devices, concerning the π–π interaction between conjugated polymer chains.

There are some excellent review articles on conjugated polymers and polymer-based solar cells.[5,6,8,11,17,24,41,42] This review aims to highlight different fabrication techniques for polymer nanostructures for the application of organic solar cells. As shown in Fig. 7, these methods are divided into subjects including polymer nanowires, nanoparticles, block copolymers, layer-by-layer deposition, nanoimprint lithography, template methods, nanoelectrodes, and porous inorganic materials. Here we mainly focus on the nanostructures of the donor materials such as P3HT. In order to make heterojunction solar cells, the acceptor materials are usually deposited on the nanostructured donor materials. A typical example is to make P3HT nanorods using templates or nanoimprint lithography, then the PCBM can be deposited on the P3HT nanorods for constructing the donor–acceptor heterojunction. Although here we only focus on the discussion of donor nanostructures, these concepts can be applied to make the acceptor nanostructures. For example, C_{60}, TiO_2 or ZnO nanorods can be generated by porous templates, followed by the spin-coating of the P3HT.[43–46]

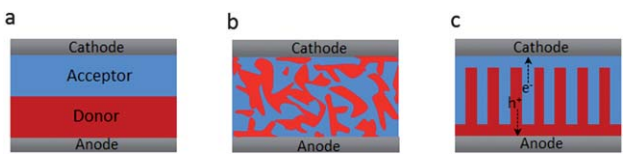

Fig. 6 Three possible donor–acceptor morphologies of organic solar cells. (a) Double layer morphology. (b) Phase-separated donor–acceptor blend morphology. (c) Ideal heterojunction morphology.

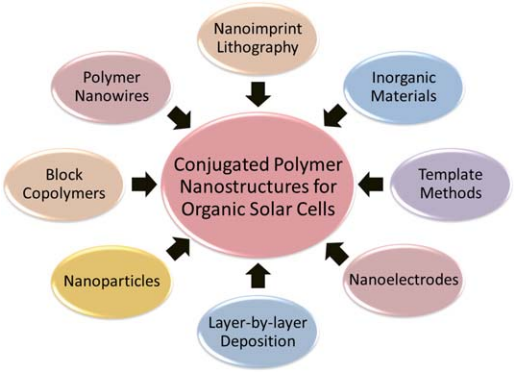

Fig. 7 Approaches to fabricate conjugated polymer nanostructures for applications in organic solar cells.

2 Strategies for fabricating polymer nanostructures

This part summarizes some common strategies and techniques for making polymer nanostructures for the application of organic solar cells. The device performance based on different nanostructures will also be presented.

2.1 Polymer nanowires

One of the most common conjugated polymer nanostructures used in organic solar cells is conjugated polymer nanowires, for they provide percolation pathways for both electrons and holes, resulting in higher device efficiency. Nanowires are sometimes called nanocylinders, nanofibers, or nanowhiskers, meaning one-dimensional nanomaterials with high aspect ratios. The advantages of using the polymer nanowires approach for solar cell devices include (a) the morphology can be controlled; (b) the widths and lengths of polymer nanowires are matched to the exciton diffusion lengths; (c) the interfacial area between donor and acceptor is large; (d) an electrically bicontinuous morphology can be obtained; (e) high absorption coefficient and high carrier mobilities can be achieved; (f) devices on plastic substrates and devices with large areas can be easily produced; (g) the difficulties of blend phase-separation phenomena can be avoided.[47,48]

Various techniques have been applied to prepare conjugated polymer nanowires. It has been found that the polymer nanowires can be simply observed by thermal annealing.[28] For example, P3HT nanowires were observed after annealing the P3HT/PCBM mixture at 120 °C for 60 min.[28] The annealing process increases the crystallinity of P3HT and enhances the demixing between P3HT and PCBM. Another simple method to generate P3HT nanowires was studied by Sun *et al.*[49] They found that P3HT nanowires and CdSe nanorods can be obtained by careful choice of the solvent used for spin-coating. 1,2,4-Trichlorobenzene (TCB), which has a high boiling point, was used as the solvent for P3HT and a fibrillar morphology was obtained. The power efficiency of the solar cell devices based on the composites of P3HT nanowires and CdSe nanorods was improved to 2.6% (AM 1.5G), compared with 1.8% where chloroform was used as the solvent and P3HT nanowires were not formed.[49]

In addition to the previously mentioned methods, the two most common ways to make conjugated polymer nanowires for the applications in organic solar cells are the whisker method and the mixed-solvent method.

2.1.1 The whisker method. The whisker method was first developed by Ihn *et al.*[50] They reported that poly(3-alkylthiophene)s may readily crystallize from dilute solutions in relatively poor solvents in the form of ribbon-shaped whiskers. The formation of whiskers is dependent on the solvent quality, temperature, and the alkyl side-chain length. The widths of the whiskers are about 15 nm and their lengths often exceed tens of microns, so very high aspect ratios are observed for the whiskers. The polymer chains made by the whisker method were found to pack with their backbones normal to the whisker direction.[50] Fig. 8 shows an example using the whisker method to make P3HT nanowires. P3HT polymers are dissolved in *p*-xylene and heated to 80 °C. The solution is later cooled down to room temperature and P3HT nanowires are formed.

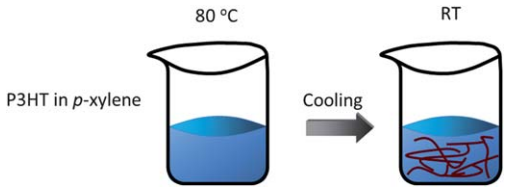

Fig. 8 Schematic illustration showing an example of using the whisker method to make P3HT nanowires. P3HT polymers are dissolved in *p*-xylene and heated to 80 °C. The solution is later cooled down to room temperature and P3HT nanowires are formed.

To address the issue of what solvents are most suitable for nanofiber formation using the whisker method, Oosterbaan *et al.* performed systematic studies of the fiber formation of regioregular poly(3-alkylthiophene)s (P3ATs) with alkyl chain lengths between 3 and 9 carbon atoms in several solvents.[51] For the aliphatic and (chlorinated) aromatic hydrocarbon solvents, the refractive index of the solvent was used to predict the feasibility of a particular solvent for the fiber formation. The effect of poly (3-alkylthiophene) (P3AT) crystallinity on the energy of the intermolecular charge-transfer state (E_{CT}) and open-circuit voltage (V_{oc}) in P3AT nanofibers:PCBM solar cells was also investigated.[52] The P3AT crystallinity can be varied by controlling the temperature. The E_{CT} was found to increase slightly with increasing side-chain length and the V_{oc} followed the same trend as E_{CT} because of the morphological changes.[52]

Using the whisker method, P3HT nanofibers are most studied compared with other P3AT nanofibers. Berson *et al.* presented a new fabrication procedure to produce highly concentrated solutions of P3HT nanofibers in *p*-xylene.[53] The concentration range of up to 2% allowed the deposition of thick films and the obtained solutions were stable for several weeks. By mixing these nanofibers with an electron acceptor such as PCBM in solution, a highly efficient active layer for organic solar cells with a PCE of up to 3.6% (AM 1.5G, 100mW cm^{-2}) was obtained without any thermal post-treatment.[53] The maximum PCE was achieved with the optimum composition of 75 wt% nanofibers and 25 wt% disorganized P3HT. It was proposed that the fraction of disorganized P3HT is probably necessary to fill the gaps in the nanostructures and intimate contact between the donor nanofibers and the acceptor domains can be ensured.[53] The device efficiency can also be improved by controlling the fiber content of the casting solution. Bertho *et al.* demonstrated that the fiber content of the P3HT-nanofiber:PCBM casting solution can be easily controlled by changing the solution temperature.[54] At a solution temperature 45 °C, a 42% fiber content of the casting solution was found and an optimal PCE of 3.2% was achieved, which was linked to the morphology of the active layer.[54]

For the P3HT nanowires/PCBM system, Kim *et al.* tried to optimize solar cells based on the P3HT nanowires *via* solution crystallization in DCM.[55] They studied the performances of the solar cell devices based on the P3HT nanowires/PCBM composites as a function of solution ageing time. The PCE of 3.23% was achieved for the devices coated with a 60 h aged P3HT nanowires/PCBM blend solution. The ageing process was thought to increase both light absorption and charge balance.

When a pure donor phase layer was inserted between the ITO/PEDOT:PSS and P3HT nanowires/PCBM layers, an even higher PCE of 3.94% was achieved.[55]

For solar cells based on the P3HT nanowires, other electron acceptors other than PCBM have also been used. Salim *et al.* reported the first application of the preassembled P3HT nanowires with poly(9,9-dioctylfluorene-*co*-benzothiadiazole) (F8BT) in all-polymer solar cells.[56] The role of the polymer nanowires on the morphology of the polymer blends was investigated. Compared with as-cast blends, an enhancement in the short-circuit current (J_{sc}) by a factor of 10 was achieved when P3HT nanowires were added into the blends with polyfluorene copolymers. A higher PCE was achieved for the solar cells comprising the nanowire blends, even compared with the thermally annealed ones. The enhanced device performance was attributed to the enhanced optical absorption and charge transport originating from the high crystallinity of the polymer nanowires.[56]

Inorganic nanorods have also been used in the solar cells based on P3AT nanowires. Jiu *et al.* demonstrated that the use of preformed poly(3-alkylthiophene) nanowires in hybrid solar cells with CdSe nanorods achieved a PCE of 1%.[57] The device performance from nanowires prepared from poly(3-butylthiophene) (P3BT) was better than that from poly(3-hexylthiophene) (P3HT). The CdSe nanorods were found to be dispersed within the interpenetrated 3-D network of interconnected polymer nanowires, which improved electron and hole transport in the hybrid film. The maximum PCE of 1.01% (AM 1.5G, 100 mW cm^{-2}) was achieved with the optimum composition of 25 wt% P3BT nanowires and 75 wt% CdSe nanorods.[57]

Other P3AT nanowires-based solar cells other than P3HT have also been studied. By using poly(3-butylthiophene) nanowires (P3BT-NW) as the donor and PCBM as the acceptor, Xin *et al.* reported that solar cells with 3.0% power conversion efficiency (AM 1.5G, 100 mW cm^{-2}, 10 mm^2 device area) was achieved.[47] The performance achieved was 1 order of magnitude higher than that from thermally induced phase-separated P3BT:PCBM blend. In their approach, P3BT-NW/PCBM nanocomposites exhibited an electrically bicontinuous morphology without going through the path of blend phase-separation phenomena. The results indicated that the P3BT NWs constitute an ideal donor component for enhanced exciton diffusion and charge transport in solar cell devices.[47] Xin *et al.* also fabricated bulk heterojunction solar cells based on blends of regioregular poly(3-butylthiophene) (P3BT) nanowires and phenyl-C_{61}-butyric acid methyl ester (PCBM) using *in situ* self-assembly of P3BT nanowires.[48] The approach of *in situ* self-assembly has the advantages of simplifying and combining the previously separate process of preparing P3BT NWs and blending with PCBM into a single process. The P3BT NWs were found to self-assemble to an interconnected network in the presence of the PCBM. The device performance was found to depend strongly on the blend composition. A maximum PCE of 2.52% was achieved at a blend ratio of 1 : 0.5 (wt : wt) P3BT : PCBM.[48]

Although a power conversion efficiency (PCE) of 3.0% is achieved from the P3BT-NW/fullerene composite,[47] the device structure was not optimized. Xin *et al.* systematically varied the morphology of P3BT-NW/fullerene composites by using a combination of thermal and solvent annealing.[58] The photovoltaic performance was found to vary with the induced structural variations. In unannealed devices, fullerene was found to disperse homogeneously in the P3BT-NW matrix and poor photovoltaic performances was obtained. The aggregation of fullerene in the interstitial spaces of the nanowire network was induced by thermal annealing and improved photovoltaic performance was obtained. The authors suggested that the best device performance can be achieved when the ideal interpenetrating network of nanowires and fullerene is maintained while avoiding the device bridging of the polymer nanowires.[58]

Of all the regioregular poly(alkylthiophene) nanowires, regioregular poly(3-pentylthiophene) (P3PT), which has odd-numbered alkyl side chains (C_nH_{2n+1}, $n = 5$), is less studied. Wu *et al.* first reported the fabrication of regioregular poly(3-pentylthiophene) (P3PT) nanowires and their applications in solar cells.[59] The P3PT nanowires with a width of 16–17 nm and aspect ratios of 70–465 were assembled from dichlorobenzene solution. The power conversion efficiency (AM 1.5G, 100 mW cm^{-2}) of bulk heterojunction solar cells based on P3PT nanowires/$PC_{71}BM$ nanocomposites was 3.33%, while the power conversion efficiency of bulk heterojunction solar cells based on P3PT/fullerene ($PC_{71}BM$) blend thin films was 3.70%.[59]

Block copolymer nanowires have also been fabricated using the whisker method. Ren *et al.* studied solution-phase self-assembled nanowires from diblock copolymer semiconductors, poly(3-butylthiophene)-*block*-poly(3-octylthiophene).[60] For the copolymer nanowires, the authors tried to control the aspect ratio of solution phase assembled nanowires and studied the effects of the aspect ratio on their properties and device performances. The aspect ratio of the diblock copolymer nanowires was controlled by the copolymer composition. The vertical charge transport of the nanowires/fullerene thin films was found to be independent of aspect ratio of the nanowires, indicating a parallel orientation of the nanowires to the underlying substrate.[60] But the power conversion efficiency of the solar cells based on nanowires/$PC_{71}BM$ nanocomposites was found to be dependent on the aspect ratio of the nanowires. A power conversion efficiency of 3.4% was achieved when the highest average aspect ratio of 260 was used. The improvement of device performance with the aspect ratio of nanowires was attributed to the increased exciton and charge photogeneration and collection in the solar cells.[60]

2.1.2 The mixed-solvent method. The second common ways to make conjugated polymer nanowires for the application of solar cells is by using mixed solvents.[61–66] In the mixed-solvent method, the polymer nanowires are driven by using a combination of good and bad solvents. The polymers are usually dissolved in a good solvent. Then a small quantity of bad solvent is added to the solution. The mixed solvent methods are based on the idea that the unfavourable interactions between the polymer chains and the bad solvent can induce the aggregation and self-assembly of the polymer chains. Therefore, the amount of the bad solvent in the solution will determine the degree of crystallization of the polymers. Fig. 9 shows an example of making P3HT nanowires using the mixed-solvent method. The P3HT polymers are first dissolved in a good solvent. After the bad solvent is added, P3HT polymers start to aggregate and P3HT nanowires are formed.

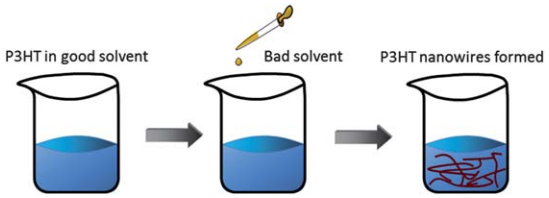

Fig. 9 Schematic illustration of using the mixed-solvent method to make P3HT nanowires. The P3HT polymers are first dissolved in a good solvent. After the bad solvent is added, P3HT polymers start to aggregate and P3HT nanowires are formed.

The mixed-solvent method was used by Kiriy *et al.* to fabricate one-dimensional polyalkylthiophene aggregation in dilute solution by adding a poor solvent to the solution.[61] Hexane, a good solvent for alkyl side chains but a poor solvent for polythiophene backbones, was used and the polyalkylthiophene formed ordered main-chain collapse driven by the solvophobic interaction. Length of the polyalkylthiophene aggregation can be adjusted by the concentration of polyalkylthiophenes or the solvent composition.[61] The solar cell performance of these polyalkylthiophene aggregations was not reported. Moulé *et al.* then used a similar mixed-solvent method to determine the agglomerated–amorphous ratio of P3HT and to control the degree of agglomeration/crystallinity of P3HT in the P3HT/PCBM solar cell mixtures.[62] The advantage of this method is that the filtering is not required to obtain pure agglomerated P3HT, and further heat-treatment of the polymer is not required. By adding nitrobenzene as the dipolar solvent, the ratio of the P3HT in the amorphous and aggregated phases was controlled and P3HT aggregates were formed. A power conversation efficiency of 4% (AM 1.5G) was achieved based on the P3HT/PCBM solar cell mixtures with no pre- or post-treatment steps.[62]

The mixed solvent method was also used by Li *et al.* to make ordered aggregates of P3HT, and the crystallinity of P3HT was substantially increased.[63] Hexane, a poor solvent for P3HT, was titrated into well-dissolved P3HT-*o*-dichlorobenzene (ODCB) solution. A power conversion efficiency of 3.9% was achieved based on a P3HT:PCBM composite using this method, almost four times than that of the pristine device.[63] Zhao *et al.* also prepared P3HT solution containing crystalline P3HT nanofibers by adding a small amount of acetone into the solution.[64] The solvatochromic phenomenon in the P3HT was observed when acetone was added, and the solution color shifted gradually from orange to dark purple with more acetone content. The best power conversion efficiency of 3.60% was achieved based on the solar cell devices with the P3HT:PCBM composites prepared from the chlorobenzene solution containing 2.5% acetone. This value was higher than 3.45% from the control device, showing that the hole transport is enhanced by adding small amount of P3HT nanofibers because of the good connectivity of P3HT nanofibers, and the demixing of PCBM is not influenced.[64]

Using the mixed solvent method, Kim *et al.* studied the sonication-assisted self-assembly of P3HT nanowires with $PC_{61}BM$ in a cosolvent system containing acetonitrile as the polar solvent.[67] The self-assembly of P3HT nanowires was found to depend on the regioregularity of P3HT, solvent polarity, and ultrasonic irradiation. A power conversion efficiency of 4.09% was achieved based on the thermally annealed solar cells having the self-assembled 98% regioregular P3HT nanowires/$PC_{61}BM$ by the sonication-assisted self-assembly.[67]

In order to prepare well-controlled nanoscale morphologies in the P3HT nanowires/PCBM film, Kim *et al.* described a two-step process.[65] The first process was the *in situ* formation of self-organized P3HT nanowires by adding the marginal solvent, cyclohexanone, to the blend solution in chlorobenzene. The second process was the nanoscale phase separation achieved by mild thermal annealing. This dual process effectively reduced the interference between P3HT crystallization and phase separation. The nanoscale PCBM domains were developed in the second step and bicontinuous percolation pathways between the P3HT and PCBM components were produced. The power conversion efficiency of 4.04% was achieved based on the P3HT nanowires/PCBM film fabricated by the two-step process, with a photocurrent density of 10.9 mA cm^{-2} and a fill factor of 62.1%.[65]

Different from previous methods, Sun *et al.* reported an unusual mixed-solvent approach to prepare P3HT nanofibers.[66] P3HT was dissolved in a large quantity of marginal solvent with a small amount of good solvent (chlorobenzene). The effects of two marginal solvents, *p*-xylene and anisole, on the morphology and solar cell performances were investigated. At room temperature, anisole has a poorer solvent quality to P3HT compared with *p*-xylene and was found to promote a higher degree formation of P3HT nanofibers. A 50% improvement of the power conversion efficiency was observed for the P3HT nanofibers by adding chlorobenzene into P3HT/anisole system than the pure anisole system.[66]

2.2 Conjugated polymer nanoparticles

Conjugated polymer nanoparticles have also been applied to fabricate organic solar cells. There are several approaches for making polymer nanoparticles including reprecipitation, emulsion polymerization, microfluidic-assisted synthesis, and miniemulsion. The reprecipitation and miniemulsion methods are the two most commonly used methods to make conjugated polymer nanoparticles.[68–70]

The reprecipitation method was first developed by Kasai *et al.*[71] The particle formation is controlled by nucleation and growth, or spinodal phase separation. The sizes of polymer nanoparticles are controlled by the water temperature and the concentration of the polymer solution. This method was used by Kurokawa *et al.* to make nanoparticles of poly(thiophene).[68] In their studies, polymer solution was injected into vigorously stirred DI water by using a microsyringe. Szymanski *et al.* used a similar reprecipitation method to make different conjugated polymer nanoparticles such as MEH-PPV.[69,70] Another modified reprecipitation method was developed by Yabu *et al.* and regular sized polymer nanoparticles were obtained.[72] In the modified method, a small amount of poor solvent (water) was slowly dropped into a polymer solution (polystyrene in THF). After the good solvent (THF) evaporated, the dissolved polymer precipitated as fine particles.[72]

The second common approach to generate conjugated polymer nanoparticles is by the miniemulsion process.[73–77] In the miniemulsion process, the polymers are first dissolved in a suitable solvent, followed by adding of water containing a small

amount of a suitable surfactant. After sonication for a short time, a homogeneous size distribution of the droplets of the resulting miniemulsion is reached, and the whole mixture is sonicated. Finally, a stable, aqueous dispersion of polymer nanoparticles is obtained after the evaporation of the organic solvent by gentle heating.

The miniemulsion technique was used by Kietzke *et al.* to prepare polyfluorene nanoparticle blends for solar cell devices.[76] The polymer used are poly(9,9-dioctylfluorene-2,7-diyl-*co*-bis-*N*,*N*′-(4-butylphenyl)-bis-*N*,*N*′-phenyl-1,4-phenylenediamine) (PFB) and poly-(9,9-dioctylfluorene-2,7-diyl-*co*-benzothiadiazole) (F8BT). They applied two different approaches which both involve using thin spin-coated layers. For the first approach, heterophase solid layers were prepared from the mixing of two dispersions of single-component nanospheres. For the second approach, each individual particle contained both polymers. Polymer solar cells based on the polymer nanoparticles made by these two methods were fabricated, and device efficiencies were found to be comparable to those of solar cells prepared from solution. The device efficiencies were also found to be independent of the choice of solvent which was used in the miniemulsion process.[76] Kietzke *et al.* also fabricated solar cells based on the single- and dual-component polymer nanoparticles to further study the dependence of the solar cell efficiency on the layer composition.[77] They found that an external quantum efficiency of 4% was achieved for the solar cell device based on polymer blend nanoparticles containing PFB:F8BT at a weight ratio of 1 : 2 in each individual nanoparticles. The authors proposed that the small exciton diffusion length of F8BT and the tendency of F8BT to penetrate the PFB phase are the most important factors for the efficiency of these devices.[77]

Using similar methods for generating polymer nanoparticles, Snaith and Friend reported an electroplating technique to form a continuous uniform film of polyfluorene nanoparticles on conductive and polymer-coated substrates.[78] By spin-coating an F8BT layer on top of the PFB:F8BT nanoparticle film, a multilayer structure was formed. A solar cell device based on the multilayer structure was fabricated, and an open-circuit voltage of 0.75 V was observed for the device based on the electroplated nanoparticles.[78] In addition to polyfluorene nanoparticles, Tada and Onoda demonstrated the preparation of stable colloidal suspensions of different materials such as C_{60}, MEH-PPV, and poly(3-alkylthiophene).[79] A small amount of solution of target materials was injected into a large amount of nonsolvents. These organic particles can be collected by electrophoretic deposition to make nanostructured films.[79]

2.3 Block copolymers

Block copolymers are polymers that consist of covalently-linked blocks, and they have aroused great interest in recent years because of their nanoscale self-assembly.[80,81] Depending on the number of blocks, the relative block volume fraction, and the interaction parameters between the blocks, block copolymers can self-assemble into a variety of ordered morphologies such as sphere, cylinder, or lamella. External fields such as electric fields or solvent annealing have been employed to orient the microdomains of block copolymers.[82–84] Block copolymers are very useful in organic solar cell applications.[85] In this review, we will focus on the use of diblock copolymers, which are comprised of two chemically distinct blocks. For the applications in organic solar cells, lamella and cylinder morphologies are usually the preferred morphologies, because they provide the percolation pathways for charge transport. As shown in Fig. 10, there are several strategies for using the block copolymers in the application of organic solar cells, which will be discussed below.

2.3.1 Donor–acceptor block copolymers. For the application of organic solar cells, the simplest case is to use a donor–acceptor block copolymer. The self-assembly of the block copolymers create the interface needed for the electron dissociations. It was demonstrated by Lindner *et al.*, who studied a single-active-layer solar cell device from block copolymers, poly(bisphenyl-4-vinylphenylamine)-*block*-poly(perylene diimide acrylate) (PvTPA-*b*-PPerAcr).[86] The electronic functionalities were attached as side groups instead of as main chains. The performance of the solar cell devices based on the block copolymers was increased by one order of magnitude with respect to efficiency compared with the devices based on the blend of the two individual segment polymers.[86] This improved performance was suggested to be caused by the larger phase-separated donor–acceptor interface in the block copolymers.[86,87]

Later, Sommer *et al.* reported the synthesis and characterization of two block copolymers, poly(bis(4-methoxyphenyl)-4′-vinylphenylamine)-*block*-poly(perylene diimide acrylat) (PvDMTPA-*b*-PPerAcr) and poly(*N*,*N*′-bis(4-methoxyphenyl)-*N*-phenyl-*N*′-4-vinylphenyl-(1,1′-biphenyl)-4,4′-diamine)-*block*-poly(perylene diimide acrylat) (PvDMTPD-*b*-PPerAcr).[87] The hole-conducting blocks bis(4-methoxyphenyl) phenylamine (DMTPA) and *N*,*N*′-bis(4-methoxyphenyl)-*N*,*N*′diphenyl-(1,1′biphenyl)-4,4′diamine (DMTPD), are more electron-rich than bisphenyl-4-vinylphenylamine (TPA). The new hole-conducting blocks were used to vary the HOMO of the donor and to improve the hole-carrier mobility. The power conversion efficiency of the solar cell based on PvDMTPA-*b*-PPerAcr was improved to 0.32%.[87]

P3HT has also been synthesized into the block copolymers for use in organic solar cells. For example, Zhang *et al.* synthesized a donor–acceptor diblock copolymer in which the electron donor block is regioregular P3HT and the electron acceptor block is poly(perylene diimide acrylate) (PPDA), a polyacrylate with pendent perylene diimide groups.[88] In the solid state, the copolymers showed efficient photoluminescence quenching, indicating the charge separation. The power conversion efficiency of the solar cell based on the block copolymer was achieved at 0.49%

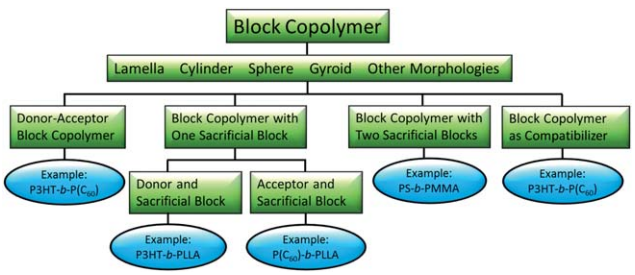

Fig. 10 Strategies for using block copolymers for organic solar cell applications.

using AM 1.5G solar simulation.[88] Lee *et al.* then synthesized a new, well-defined diblock copolymer (P3HT-*b*-C_{60}) based on regioregular P3HT and fullerene.[89] The P3HT-*b*-C_{60} showed phase separation when the block copolymer was thermally annealed. Complete photoluminescence quenching of the P3HT-*b*-C_{60} film was observed, while the P3HT/PCBM blend still showed some photoluminescence, indicating that the charge transfer between P3HT and C_{60} are more effectively in the P3HT-*b*-C_{60} diblock copolymer than that in the P3HT/PCBM blend. Tao *et al.* reported the synthesis of rod–coil block copolymers poly(3-hexylthiophene)-*b*-poly(*n*-butyl acrylatestat-acrylate perylene) containing electron donor poly(3-hexylthiophene) and acceptor perylene.[90] The self-assembled morphology of the block copolymers and the performances of the solar cells based on the self-assembled block copolymers were studied. The authors concluded that the device performance can be significantly improved from well-defined interfaces but poorly organized nanostructures.[90]

2.3.2 Block copolymer with one sacrificial block. The second strategy for the application of block copolymers in organic solar cells is to use a diblock copolymer with one conjugated block and one sacrificial block. This strategy relies on the self-organization of block copolymers to generate idealized morphologies. Upon removal of the sacrificial block after the microphase separation, nanopores or nanogaps are formed with the presence of the conjugated block (donor).[91] Then the second active material (acceptor) can be filled into the nanopores or nanogaps to form an ordered bulk heterojunction. The most common examples are based on the use of block copolymers with one block of P3HT and a sacrificial block.[92] McCullough *et al.* discovered that end-functionalized P3HTs can be synthesized with low polydispersity using a catalyst-transfer polycondensation method.[93,94] They further showed that block copolymers of P3HT can be synthesized by using the end-functionalized P3HTs *via* atom transfer radical polymerization (ATRP).[95] Using a similar method combined with anionic polymerization, Dai *et al.* synthesized copolymers consisting of P3HT and poly(2-vinylpyridine) (P2VP) that microphase-separated and self-assembled into different nanostructures of sphere, cylinder, and lamella. Different nanofiber structures were also observed depending on the volume fraction of the P2VP block.[96]

For the application of organic solar cells, Botiz *et al.* demonstrated the synthesis of poly(3-hexylthiophene)-*block*-poly(L-lactide) (P3HT-*b*-PLLA) linear diblock copolymer as a structure-directing agent for patterning active materials into ordered nanostructures.[97] The block copolymers self-assembled to form a lamellar morphology, determined by the molecular weights of the two blocks. The biodegradable PLLA block was selectively removed by NaOH solution after the ordered microphase-separated morphology was obtained. Acceptor material fullerene hydroxide (C_{60}) was then filled the gaps between the P3HT domains by dip-coating technique.[97] One challenge using this strategy is the lateral collapse of the resulting P3HT nanostructures after removing the PLLA. Botiz *et al.* further addressed this issue by proposing that collapse and the subsequent aggregation of the P3HT domain is because of the capillary forces present between the nanodomains.[98] They applied different drying approaches to control the surface tension forces generated during the liquid evaporation process. A reduction in domain collapse was observed and the molecular ordering in the plane perpendicular to the substrate was improved.[98]

2.3.3 Block copolymer with two sacrificial blocks. Block copolymers can also be used simply as a template, where both blocks in a diblock copolymer are sacrificial blocks. One of the blocks will be selectively removed to create spaces that could be filled with the conjugated polymers as the donor. The second sacrificial blocks will then be removed, followed by the deposition of the acceptor materials. Therefore, the block copolymers are not present in the final devices. The advantage of this strategy is that well-ordered block copolymers such as the common poly(styrene)-*block*-poly(methyl methacrylate) (PS-*b*-PMMA) can be used and general methods to align the block copolymer domains can be applied. In addition, the problem that the crystalline behaviour of most conjugated polymers can affect the microphase-separation of block copolymers is avoided by using amorphous block copolymers as templates.

Conducting polymer nanorods were prepared by Lee *et al.*, who used a porous diblock copolymer as a template.[99] In their work, a mixture of poly(styrene)-*block*-poly(methyl methacrylate) (PS-*b*-PMMA) and a poly(methyl methacrylate) (PMMA) homopolymer is spin-coated onto a random copolymer-coated ITO substrate. Nanopores were generated after the PMMA homopolymer was removed using a selective solvent. The arrays of conducting polypyrrole (PPy) nanorods were fabricated directly on the indium-tin oxide coated glass by an electropolymerization.[99] The PPy nanorods were shown to have much higher conductivity than that of thin PPy films, which is caused by the high degree of chain orientation. The block copolymer template was removed by using a suitable solvent, resulting in self-supporting arrays of conducting polymers oriented normal to the substrate surface. This method will be useful considering the well-controlled conjugated polymer nanorods. The block copolymer templates can be filled with other conjugated polymers such as P3HT, and solar cells devices can be made after the removing of the second sacrificial block, followed by the evaporation of other active materials such as PCBM.

2.3.4 Block copolymers as compatibilizers. Instead of being used as the active materials, block copolymers can be used as compatibilizers in organic solar cells. In the P3HT/PCBM system, a thermal annealing step above the glass transition temperature (T_g) of the active material is usually applied to improve the device performance.[27,28] But phase segregation also occurs during the annealing process, affecting the resultant efficiency. The block copolymers can be used as compatibilizers to lower the interfacial energy between donor acceptor domains and can affect the phase segregation behaviour of the active materials.

Amphiphilic diblock copolymers incorporating fullerene and P3HT macromonomer was synthesized by Sivula *et al.* for their uses as compatibilizers in P3HT/PCBM based solar cells.[26] Phase segregation of P3HT and PCBM domains were found to be altered and even prevented by using the compatibilizers. Yang *et al.* also synthesized rod–coil block copolymers based on P3HT containing C_{60} chromophores (P3HT-*b*-P(SxAy)-C_{60}) and used the block copolymer as a surfactant for the P3HT/PCBM based

solar cells.[100] The interfacial morphology between P3HT and PCBM domains was altered by adding a small amount of the block copolymer (P3HT-*b*-P(SxAy)-C_{60}). The efficiency of the solar cell was improved to 3.5%, which was 35% increase compared with the standard device without adding the block copolymer.[100]

2.4 Layer-by-layer deposition

Organic solar cells based on multi-layered small molecule films have been fabricated using vacuum deposition. For example, the power conversion efficiency of 3.6% was achieved from a simple donor–acceptor bilayer cell based on copper phthalocyanine (CuPc) and fullerene (C_{60}).[101] Even though the vacuum deposition technique is useful for precisely controlling the film thickness, this technique usually requires high-vacuum and high temperatures conditions, which is not suitable for polymer materials.[102] Therefore, multi-layered solar cells based on polymers are relatively less studied. In addition, it is usually difficult to find suitable selective solvents for making multi-layered polymer films to avoid the dissolving problem.

Layer-by-layer (LbL) approaches have been one of the best methods to generate conductive multilayer films based on conjugated polymers.[103–106] These multilayer films are fabricated in organic solvents and are useful in different optoelectronic applications such as the organic solar cells. Liang *et al.* reported the synthesis and fabrication of hybrid multilayer thin films of poly(*p*-phenylenevinylene)s (PPVs), and CdSe nanoparticles by using the layer-by-layer assembly approach.[106] This method enables the preparation of hybrid thin films with great stability through covalent coupling reactions between polymers and nanoparticles. The power conversion efficiency of 0.71% (10 mW cm^{-2}) was achieved from the solar cells based on the PPV/CdSe nanocomposites.[106] Solar cells based on the self-assembled layers of functional polymers and inorganic particles using the layer-by-layer method was also demonstrated by Kniprath *et al.*[107] Alternating layers of the polythiophene derivative, poly(2,3-thienyl-ethoxy-4-butylsulfonate) (PTEBS), and TiO_2 nanoparticles were prepared using the layer-by-layer methods. Solar cells based on the composites films were fabricated and stable photovoltaic behavior was observed with photovoltages of up to 0.9 V.[107] Hybrid films of polymers and lead selenide nanocrystals (PbSe-NCs) using the layer-by-layer deposition technique was reported by Vercelli *et al.*[108] PbSe-NCs and sulfonate-, carboxylate-, and pyridine-based polymers were alternately deposited on ITO-glass surfaces. The hybrid film was expected to be useful for organic-inorganic solar cells in the infrared region of the solar spectrum.[108]

Benten *et al.* reported the preparation of poly(*p*-phenylenevinylene) (PPV) by using the layer-by-layer deposition of the PPV precursor cation and poly(sodium 4-styrenesulfonate) (PSS) and studied their applications in solar cells.[102] Multilayer polymer solar cells were fabricated based on the layer-by-layer assembled PPV layer. In their work, the PEDOT:PSS spin-coated film was cross-linked by gelation, yielding insoluble film in the polyelectrolyte aqueous solutions. The best power conversion efficiency of the solar cells based on PEDOT:PSS/PPV/C_{60} was achieved at 0.26% (AM 1.5G, 100mW cm^{-2}, air), where the thickness of the PPV layer was 11 nm, comparable to the diffusion length of the PPV singlet exciton.[102]

2.5 Nanoimprint lithography

As shown in Fig. 11, nanoimprint lithography (NIL) uses a mold with nanostructures that can be transferred into a polymer by imprinting the mold onto the polymer.[109] The fabrication of the nanostructures on the mold is mostly done by e-beam lithography and is time-consuming and expensive. But these molds can be repeatedly used, so the mold can be applied in an inexpensive and fast process. The NIL process can be used for small areas, but roll-to-roll processing and imprinting for large area are also feasible. NIL has been employed by several groups to produce nanostructures in the application of organic solar cells.[110–112] For polymer-based solar cell devices, the device performances are improved when nanoscale structures are imprinted into the donor polymer film, followed by the evaporating or spin-coating of acceptor materials.

Nanopatterns of polythiophene derivatives on flexible plastic were demonstrated by Kim *et al.* using the nanoimprint lithography.[110] Solar cell devices were fabricated after spin-coating PCBM and evaporating Al. The short-circuit current of the nanoimprinted devices was shown to increase with the interfacial area of the structures. The fill factor and power conversion efficiency also increased with the interfacial area.[110]

High density periodic P3HT nanopillars ($\sim 10^{10}$ cm^{-2}) were reported by Aryal *et al.* using nanoimprint lithography.[111] A large-scale nanoporous Si mold was obtained by using an anodic alumina template as a mask for a two-step plasma etching process. The pores in the Si mold were 50–80 nm wide and 100–900 nm deep and the pore depth and profile can be controlled by adjusting the plasma etching conditions such as Cl_2 : Ar ratio, time, pressure, and bias power. Ordered and high density polymer nanopillars including poly(methyl methacrylate) (PMMA) and P3HT were fabricated by this method.[111] The imprinted P3HT nanopillars were then used for organic solar cell devices followed by depositing PCBM on top of the nanostructures. For the purpose of comparison, double layer nonpatterned solar cell devices without the imprinting steps using similar process were fabricated. The power conversion efficiency (AM 1.5G, 100 mW cm^{-2}) was improved by 78% from the solar cell devices built on imprinted P3HT pillars compared with the devices of the non-patterned layer. The fill factor and short-circuit current also showed 38% and 20% increases, respectively. The authors concluded that the main reason for the improved performance of the solar cell devices was due to the well-controlled interdigitized

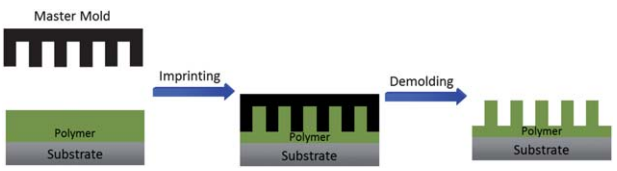

Fig. 11 Schematic illustration of using the nanoimprint lithography to make polymer nanostructures. A polymer film is first coated on a substrate. A master mold is used to imprint the polymer film at elevated temperatures to transfer the patterns. Polymer nanostructures are released after the demolding process.

heterojunction morphology which allowed more efficient charge transport and exciton dissociation.[111]

For the imprinted P3HT nanostructures, Aryal *et al.*, also studied the crystallization and chain orientation by using the out-of-plane and in-plane grazing incident X-ray diffraction.[113] The geometry (gratings or pillars) of these nanostructures was shown to have a strong influence on the 3D chain alignment of the nanostructures. The chain orientations inside nanoimprinted P3HT gratings and nanopillars were proved to be vertical by in-plane and out-of-plane grazing incidence X-ray diffraction (GIXRD) measurement.[113] The chain alignment was proposed to be induced by the nanoconfinement effect during the imprinting process through π–π interaction and the hydrophobic interaction between polymer chains and the surfaces of the molding materials. The vertical chain alignment of P3HT chains in both nanogratings and nanopillars also indicate their potentials for improving charge transport and solar cell devices compared with bulk heterojunction solar cells.[113]

In addition to P3HT nanopillars, nanoimprinted P3HT nanogratings were demonstrated by Zhou *et al.*[114] The nanoimprinted P3HT nanogratings were fabricated by imprinting a P3HT film using a Si mold gratings of 100 nm in width, 100 nm in depth, and 200 nm in pitch. PCBM was then spin-coated on top of the nanograting as the electron transport material. An orthogonal solvent (dichloromethane) that dissolves PCBM well but not the P3HT was used to allow the stacking of PCBM on top of the P3HT nanostructures, resulting in nondistortion of the nanostructures. For comparison studies, two types of nonpatterned films of P3HT and PCBM were also fabricated as solar cell devices. The first type of nonpatterned film was made by spinning a 50 nm PCBM layer on top of an 85 nm thick P3HT layer. Lee *et al.* have shown that this kind of film is not a bilayer, but an intermixed heterojunciton.[37] The second type of nonpatterned film was made by spin-coating a mixture of P3HT/PCBM (1 : 0.9) onto the substrate. The power conversion efficiency (AM 1.5G, 100 mW cm^{-2}) of the solar cell with P3HT nanogratings was higher than those with the nonpatterned films.[114] The fill factor and short-circuit current also increased compared with those of the bilayer and blended solar cells. The authors concluded that the improved performance in P3HT nanograting devices was due to the better chain alignment in P3HT nanogratings and the increase in the interfacial area. The favorable 3D chain alignment enables high mobility, resulting in improved current density, fill factor, and efficiency of the nanoimprinted solar cells. The authors also proposed that better device performance can be expected by increasing the density and the aspect ratio of nanogratings.[114]

To further improve the performance of P3HT nanogratings based solar cells, Yang *et al.* used oblique deposition to deposit C_{60} into the P3HT nanogratings to have good infiltration of C_{60} into the nanoimprinted P3HT nanogratings.[115] The evaporation angle of C_{60} was found to affect the uniformity and step coverage of C_{60} infiltration into the P3HT nanostructures. At the optimal condition for the C_{60} deposition filling, increased exciton dissociation rate at the larger P3HT-C_{60} interfacial area was achieved and the power conversion efficiency was observed to increase 50%, compared with flat bilayer devices. The authors also expected that there will be 200% enhancement in power conversion efficiency of the solar cell devices if the P3HT gratings can be twice as their width.[115]

Nanoimprinting was combined with lamination technique by Wiedemann *et al.* to make nanostructured bilayer devices.[116] In their work, P3HT was nanoimprinted using an anodic aluminum oxide as a stamp. PCBM was then deposited *via* a lift-off lamination technique.[116] Instead of forming the P3HT nanostructures first followed by depositing PCBM, Na *et al.* used a soft lithographic approach to prepare periodic patterned P3HT/PCBM structures.[117] Photo-induced surface-relief gratings on azo polymer films and poly(dimethylsiloxane) were used as a master and stamp. The power conversion efficiency of the patterned devices was 4.02%, compared with 3.56% from the unpatterned devices.[117] To avoid the nanoimprinting process at high temperatures, Shih *et al.* used textured Si wafer as a stamp to nanoimprint P3HT:PCBM blends at room temperature, and the V_{oc}, J_{sc}, and FF of the nanoimprinted devices was found to increase by 50%.[118]

To achieve the interpenetrating nanostructures, He *et al.* demonstrated a double nanoimprinting method to create nanopatterned polymer blends with features in the 25 to 200 nm size range.[119] The solar cell devices based on the nanostructured polymer blends of poly((9,9-dioctylfluorene)-2,7-diyl-alt-[4,7-bis (3-hexylthien-5-yl)-2,1,3-benzothiadiazole]-2′,2″-diyl) (F8TBT)/poly(3-hexylthiophene) (P3HT) were fabricated and the influence of feature size on device performance was investigated. The solar cell devices were shown to have extremely high densities (10^{14} mm^{-2}) of interpenetrating nanoscale columnar features in the active polymer layer.[119] The power conversion efficiency of the solar cell was improved to 1.9%, primarily due to the improved fill factor over that from the solution demixed device. The poorly controlled morphology formed from the demixed polymer blend layer was considered to cause the avoidance of locally trapped photogenerated charges, resulting in lower efficiency.[119] The same technique was also applied to polymer-fullerene based solar cell devices.[112] The AFM and SEM results showed that the features in the polymer mold used in the second imprinting process were only slightly distorted during imprinting steps. The performances of the solar cell devices using P3HT or F8TBT as the donor materials and PCBM as the acceptor material were investigated. In both cases, the performances of the devices were influenced by the feature size and the interfacial area.[112] Different from other imprinting methods, which have the disadvantages of rather large imprinted feature sizes and high temperature deposition process, the advantage of the new double nanoimprinting method is that the pure form of any materials can be used. The requirement for the donor and acceptor materials is that they have a small difference in glass transition temperature (T_g), melting temperature (T_m), or solubility in selective solvents. Otherwise, the first imprint might be erased during the second imprinting step. An additional advantage of this double nanoimprint method is that both donor and acceptor layers can completely cover the electrodes.[112,119]

The most popular choices for the donor and acceptor in the nanoimprinting method are still P3HT and PCBM. Instead of using PCBM as the electron acceptor, *N*,*N*′-ditridecyl-3,4,9,10-perylenetetracarboxylic diimide (PTCDI-C_{13}) was used by Cheyns *et al.* They first obtained trenches of poly(3-hexylthiophene) (P3HT) with feature size down to 50 nm and aspect ratio up to 2 by nanoimprinting.[109] Then the electron acceptor (PTCDI-C_{13}) was deposited from the vapor phase. Zinc oxide

(ZnO) nanoparticles was later spin-coated on top to reduce the roughness of the layered structures. A 2.5-fold enhancement of the short-circuit current was observed in the nanoimprinted devices compared with the planar devices.[109] Another electron acceptor 4,7-bis(2-(1-ethylhexyl-4,5-dicyano-imidazol-2-yl) vinyl)benzo[c]1,2,5-thiadiazole (EV-BT) was used by Zeng *et al.*[120] They applied nanoimprinting for bilayer solar cells using P3HT as the electron donor and EV-BT as the electron acceptor. The power conversion efficiency of the devices was increased to 0.3% for the nanoimprinting devices, compared with 0.2% for the simple bilayer device.[120]

2.6 Template methods

Nanoporous templates have been widely used to make one-dimensional polymer nanostructures.[121–127] Template-based methods represent straightforward routes to make nanomaterials, in which the template is simply used as a scaffold, and the materials are fabricated and shaped by the geometry of the template. Since the templates consist of cylindrical pores of uniform diameter, monodisperse nanocylinders of the desired material, whose dimensions can be carefully controlled, are obtained in high yield within the pores of the template material.[125] Another advantage of using the template method is that the placement and dimensions of different components of the nanomaterials can be controlled. Depending on the material, the chemistry of the pores wall, and other operating parameters, these nanocylinders may be solid (a nanorod) or hollow (a nanotube).[123] Fig. 12 describes the basic concept of using the template method. Different materials, such as polymers, can be introduced into the nanopores of the templates by wetting the pore walls of the porous template.[128] The surface energy of the wall is usually high and the precursor materials cover the surface of the walls to reduce the surface energy by a simple wetting process. The nanomaterials can remain inside the pores of the templates or they can be released and collected by removing the template selectively.

Various materials have been used as the porous templates, but ion-track-etched membranes and anodic aluminum oxide (AAO) templates are the most commonly employed.[129] Ion-tracked membranes are commercially available as filters in a wide variety of pore sizes.[130] They are usually prepared from either polyester or polycarbonate thin films with pore diameters ranging from 10 to 2000 nm. However, the track-etched membranes have low porosities and contain randomly distributed nanochannels across the membrane surface. In addition, the random nature of pore formation during this process can result in a large number of intersecting pores that will harmfully affect the homogeneity, number, and sizes of the synthesized nanomaterials.[125]

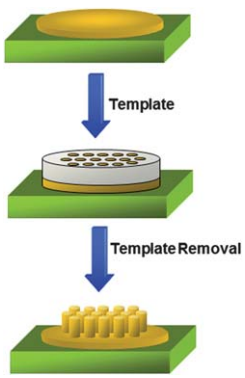

Fig. 12 Schematic illustration of using the template method to make polymer nanostructures. A polymer film is first deposited on a substrate. Then a porous template is brought into contact with the template. Polymers are able to wet the surface of the nanopores of the template by a capillary force *via* thermal annealing. After removing the template by a selective etching solution, polymer nanostructures are generated.

Another important template is anodic aluminum oxide (AAO) template which is prepared electrochemically from aluminum. The popularity of the AAO template is because of its exceptional thermal stabilities, ease of fabrication, and its regular pore diameter and pore length.[131] The AAO templates typically contain high porosities, and the pores are arranged in a hexagonal array. Pore densities as high as 10^{11} pores per square centimetre can be achieved, and typical membrane thickness can range from 10 to 100 μm.[132] AAO templates of many diameters (5–267nm) can be synthesized following the two-step anodization process established by Masuda and co-workers in which nano-sized pores are grown in an insulating oxide film of alumina.[133,134]

The template method usually requires removal of the template with selective etching solution such as weak acid or weak base. But a major challenge associated with these nanostructures is associated with their lateral collapse, which is related to the high aspect ratio of the nanostructures or the capillary force caused by the evaporation of solvent.[135,136] A freeze drying technique has been applied to remove the aqueous medium after the etching process to prevent the lateral collapse of the nanostructures.[137]

Polythiophene nanotube films were prepared by Cao *et al.* using the anodic aluminium oxide template.[138] A gold layer was first deposited onto one side of the alumina membrane template with a pore size of 20 nm. Then an ITO layer was contacted closely to the gold layer as a current collector. By direct oxidation of thiophene in boron trifluoride diethyl etherate (BFEE) solution, polythiophene nanotubes were synthesized in the nanopores of the AAO template.[138] After dissolving the template in 1M KOH solution, the aligned nanotube film was obtained. In their work, surface photovoltage spectrum (SPS) and field-induced surface photovoltage spectrum (FISPS) were used to investigate the electronic structure and the charge behaviour of the polythiophene nanotube films. They observed two extra photovoltaic responses in the near-IR region, besides the intrinsic π–π^* transition of polythiophene chains. From the principle of FISPS and the band theory, the new responses were attributed to the charged surface electronic states, which were caused by the interaction between the nanotubes and the oxygen absorbed on the surface.[138] Electrochemical polymerization was used by Huesmann *et al.*, to synthesize polythiophene with AAO templates.[139] They showed that geometry of the prepared nanostructures can be controlled by the hydrophobic side-chains, such as 3-hexyl and 3-(2-ethyl)hexyl.

Wang *et al.* reported the use of porous alumina templates to fabricate ordered arrays of core-shell P3HT and PCBM for the use in organic solar cells.[140] The P3HT/PCBM film with a thickness of 120 nm was first spin-coated onto an ITO substrate. An AAO template was then placed on top of the P3HT/PCBM film. After annealing in an oven under vacuum for 6 h, core-shell

P3HT/PCBM composite nanorods were formed. The template was dissolved by using 10 wt% NaOH solution and the nanorod arrays were released. For the solar cell devices using the P3HT/PCBM nanorods at a 1 : 0.6 ratio (w/w), the values of PCE and J_{sc} were 2.0% and 8.7 mA cm^{-2}, respectively.[140] The performance of the devices annealed at 120 °C was higher than that at 100 °C because the phase separation of the nanorods at higher temperatures was more complete, resulting in better device performance. The annealing effect induced the increase in the transport properties, the degree of crystallization, and the light absorption of the P3HT-rich region of the solar cells devices.[140]

In addition to the normal solar cell devices, Wang *et al.* also fabricated inverted heterojunction solar cell devices incorporating the core/shell P3HT/PCBM nanorod arrays.[141] The efficiencies of these core/shell nanorod inverted solar cells were higher than those of the corresponding conventional inverted bulk heterojunction solar cell devices. The hole mobility of the optimized nanorod arrays was over one order greater than that of the conventional bulk heterojunction structure. The core-shell nanorods provided a more efficient charge transport for the devices, resulting in a higher short-circuit current density and power conversion efficiency.[141]

Using the AAO template, Kim *et al.* demonstrated the fabrication of P3HT nanorods which were aligned perpendicular to the ITO substrate.[142] The AAO membranes with a diameter of 50 nm, an aspect ratio of 3, and an interpore size of 100 nm were synthesized by anodization of an aluminium sheet at 40 V in 0.3 M oxalic acid and were used as the templates. For the infiltration of the P3HT chains into the nanopores of the AAO templates, an AAO template was placed on top of a P3HT film and was heated to 250 °C for 30 min under vacuum. This temperature was used because it is well above the melting temperature of P3HT. The P3HT chains were drawn into the nanopores of the template by capillary action. The template was then removed by copper chloride ($CuCl_2$) and sodium hydroxide (NaOH) solution.[142] They found that the chain orientations of P3HT inside the nanorods were aligned in the direction normal to the pore wall of the AAO templates. The electrical conductivity of the P3HT nanorods was enhanced up to ten times compared with the conductivity of the continuous P3HT film, mainly due to the preferred crystalline orientation. The power conversion efficiency of the solar cell devices using P3HT nanorods also increased from 0.17% to 1.12% compared with devices using planar P3HT film. This 6.6 fold increase of efficiency was attributed to the conductivity enhancement afforded by the nanorods, more efficient charge separation, and a greater interface area between the donor and acceptor materials.[142]

Instead of the AAO templates, Jeon *et al.* used polycarbonate and PET membrane films as templates to make nanostructures of poly(3-octylthiophene) (P3OT) and fullerene.[143] P3OT was synthesized in the micropores of the membranes. The power conversion efficiency of the heterojunction solar cells devices was increased with increasing pore content.[143]

2.7 Nanoelectrodes

Conjugated polymer nanostructures can be made based on patterned nanoelectrodes. Most works related to this topic are based on the formation of nanorods of the anode, usually indium tin oxide (ITO). The active polymer layers are then deposited on top of the patterned nanoelectrodes, and conjugated polymer nanostructures can be generated whose geometry is based on the underlying nanoelectrodes. To obtain better device performance using this strategy, one usually has to deal with the problem of the incomplete filling of the polymers into the space created by the nanoelectrodes.[144]

An oblique electron-beam evaporation method was demonstrated by Yu *et al.* to fabricate indium-tin-oxide (ITO) nanorods.[145] The randomly oriented ITO nanorods were deposited on an ITO-coated glass substrate. After spin-coating of the hole-transport layer of PEDOT:PSS, a mixture of regioregular P3HT and PCBM with a weight ratio of 1 : 1 was used as the active layer. In this work, a small nitrogen flow was introduced in order to facilitate the segregation of indium during the nucleation process, and the resulting column growth of the ITO nanorods in an oxygen-deficient environment was therefore promoted.[146] The performance of the solar cells with ITO nanorods was compared with that of the conventional solar cells. The results showed that the solar cells with ITO nanorods represented an enhancement factor of up to 10% compared with a conventional solar cell under the AM 1.5G conditions.[145] Instead of spin-coating, Hsu *et al.* also used electrochemical deposition to deposit PEDOT:PSS onto the ITO nanoelectrodes.[146] The P3HT and PCBM mixture was then spin-coated onto the PEDOT layer for the fabrication of the solar cell devices. The performance of the solar cells with nanoelectrodes was compared with solar cells with planar electrodes, and a PCE of 3.02% was achieved for the solar cell devices with the ITO nanoelectrodes.[146]

ITO nanoelectrodes can also be fabricated by using a glancing angle deposition technique.[147] In this deposition process, the substrate is oriented at an oblique angle with respect to the incident vapour flux. After the fabrication of ITO nanoelectrodes, PEDOT:PSS and P3HT/PCBM (1 : 1 in weight ratio) were spin-coated on the substrate followed by the evaporation of aluminium. The power conversion efficiency of solar cells with the ITO nanorods was 2.2% which was a third greater than that of solar cells with a commercial ITO.[147] In addition, a silica capping technique was used to prevent electrical shorts and to reduce series resistance in the ITO nanorods-based solar cells. By using this capping technique, a further improved power conversion efficiency of 2.5% was observed.[147]

Using similar concepts, Fung *et al.* demonstrated the deposition of ITO nanorods on glass and glass/ITO substrates using electron-beam deposition and sputtering methods.[148] The deposition times for both methods were very short and the substrate was not necessary to be tilted. After spin-coating PEDOT:PSS and P3HT/PCBM (1 : 1 in weight ratio) followed by the evaporation of aluminium, solar cells using the ITO nanorods were prepared. The power conversion efficiency of solar cells with the bare ITO film is 2.1%. This value was significantly increased to 3.2% by using the solar cells with the sputtered ITO nanorods on an ITO film.[148]

2.8 Porous inorganic materials

Porous inorganic materials such as titania (TiO_2) provide a convenient way to make conjugated polymer nanomaterials. The conjugated polymers are synthesized or infiltrated into the

nanopores of the porous inorganic materials. The advantage of using this method is that the fabricated polymer nanomaterials do not need to be released from the inorganic materials because titania or some other inorganic materials already serve the function as the electron acceptor. This simplified coating process can avoid the problem that the conjugated polymers may collapse or distort during the later coating or imprinting process of the acceptor materials.[112]

Coakley *et al.* reported the preparation of films of titania with a uniform distribution of pores sizes by dip coating the substrates with a solution of a titania sol–gel precursor followed by calcination at temperatures in the range of 400–450 °C.[149] A poly (ethylene oxide)-poly(propylene oxide)-poly(ethylene oxide) triblock copolymer was used as the structure-directing agent. The nanopores in the porous titania was filled with regioregular P3HT by spin-casting a film of P3HT followed by heating at temperatures in the range of 100–200 °C. The amount of polymer that can be filled into the titania films depends on the temperature that is used for infiltration. Electron transfer from the polymer to the titania was suggested from the PL measurement. Later, Coakley *et al.* fabricated solar cells based on the mesoporous titania/infiltrated-P3HT.[150] The pore size of the mesoporous titania films is slightly less than 10 nm, which is close to the exciton diffusion length for many conjugated polymers. The power conversion efficiency of 1.5% was achieved under monochromatic 514 nm light based on the mesoporous titania/P3HT composites.[150]

Porous titania with typically 33% volume can be produced by using the poly(ethylene oxide)-poly(propylene oxide)-poly (ethylene oxide) triblock copolymer as the structure-directing agent.[149] This ratio resulted in the maximum external quantum efficiency of 10%. To increase the ratio of the nanopores in the titania film, Wang *et al.* prepared titania interconnected network structure with large pores using polystyrene-*block*-polyethylene oxide (PS-*b*-PEO) diblock copolymer as the templating agent.[151,152] The pore size can be controlled by the amount of Ti precursor. Poly(2-methoxy-5-(2′-ethyl-hexyloxy)-phenylene vinylene) (MEH-PPV) was infiltrated into the nanoporous titania and solar cell devices were fabricated. The device performance was improved with a short-circuit current of 3.25 mA cm^{-2} under AM 1.5 solar illumination.[151]

Well-ordered nanoporous titania can be fabricated by using 2D surface relief gratings (SRGs) on polymer films as a template, as reported by Kim *et al.*[153] In their work, solution of MEH-PPV in chlorobenzene was spin-coated onto the nanoporous titania followed by a baking process. The efficiency of the solar cells was increased from 0.05% for the flat titania film to 0.21% for the well-ordered nanoporous titania film. Another way to make highly ordered nanoporous titaina was demonstrated by Her *et al.*, who applied the nanoimprinting method.[154] The well-ordered nanoporous titania was fabricated by embossing the sol–gel mixture of titanium ethoxide with an array of PMMA nanopoles, followed by a sintering process at 500 °C. P3HT was used as the electron donor and was spin-coated onto the nanoporous titania. The power conversion efficiency was improved to 0.16% (AM 1.5G, 100 mW cm^{-2}) for the solar cells based on nanostructured titania/P3HT composites, compared with 0.09% for the solar cells based on flat titania films.[154]

3 Conclusions and outlook

Polymer-based solar cells have attracted considerable interest in recent years because of their low cost and easy fabrication process. To achieve the goal of commercialization, researchers have been working on many approaches to improve the device performance. Nanostructures provide large donor–acceptor interfaces for effective exciton dissociation and continuous paths for efficient charge transport. In this review, we provide an overview of different techniques for fabricating conjugated polymer nanostructures for the application in organic solar cells. Novel techniques or combination of fabrication techniques are expected to be developed to optimize the device performance. Although significant processes have been made in this field by using conjugated polymer nanostructures, there are still many challenges to overcome. The molecular orientations and conformations in the nanostructures are different from those in the bulk, especially when the size of the geometry is close to several nanometres. It is necessary to understand the dependence of the optoelectronic properties of the conjugated polymers on the size of the geometry in the molecule level. In addition, the arrangement of the donor and the acceptor at the interface requires precise control by manipulating factors such as the interfacial interaction. The optimized device performance will rely on the interdisciplinary work involving material synthesis, morphology control, structure design, and device fabrication. With these efforts, 10% or higher efficiencies are achievable for polymer solar cells to be a renewable energy source.

Acknowledgements

We thank the National Science Council of the Republic of China for financial support.

References and notes

1 M. Gratzel, *Chem. Lett.*, 2005, **34**, 8–13.
2 P. V. Kamat, *J. Phys. Chem. C*, 2007, **111**, 2834–2860.
3 A. Shah, P. Torres, R. Tscharner, N. Wyrsch and H. Keppner, *Science*, 1999, **285**, 692–698.
4 A. Goetzberger, C. Hebling and H. W. Schock, *Mater. Sci. Eng., R*, 2003, **40**, 1–46.
5 S. Gunes, H. Neugebauer and N. S. Sariciftci, *Chem. Rev.*, 2007, **107**, 1324–1338.
6 B. C. Thompson and J. M. J. Frechet, *Angew. Chem., Int. Ed.*, 2008, **47**, 58–77.
7 M. Yan, L. J. Rothberg, E. W. Kwock and T. M. Miller, *Phys. Rev. Lett.*, 1995, **75**, 1992–1995.
8 Y. J. Cheng, S. H. Yang and C. S. Hsu, *Chem. Rev.*, 2009, **109**, 5868–5923.
9 E. Bundgaard and F. C. Krebs, *Sol. Energy Mater. Sol. Cells*, 2007, **91**, 954–985.
10 F. C. Krebs, *Sol. Energy Mater. Sol. Cells*, 2009, **93**, 394–412.
11 K. M. Coakley and M. D. McGehee, *Chem. Mater.*, 2004, **16**, 4533–4542.
12 R. H. Friend, R. W. Gymer, A. B. Holmes, J. H. Burroughes, R. N. Marks, C. Taliani, D. D. C. Bradley, D. A. Dos Santos, J. L. Bredas, M. Logdlund and W. R. Salaneck, *Nature*, 1999, **397**, 121–128.
13 A. Kraft, A. C. Grimsdale and A. B. Holmes, *Angew. Chem., Int. Ed.*, 1998, **37**, 402–428.
14 T. D. Nielsen, C. Cruickshank, S. Foged, J. Thorsen and F. C. Krebs, *Sol. Energy Mater. Sol. Cells*, 2010, **94**, 1553–1571.
15 J. Rostalski and D. Meissner, *Sol. Energy Mater. Sol. Cells*, 2000, **61**, 87–95.

16 A. Gadisa, M. Svensson, M. R. Andersson and O. Inganas, *Appl. Phys. Lett.*, 2004, **84**, 1609–1611.
17 G. Dennler, M. C. Scharber and C. J. Brabec, *Adv. Mater.*, 2009, **21**, 1323–1338.
18 H. Sirringhaus, N. Tessler and R. H. Friend, *Science*, 1998, **280**, 1741–1744.
19 V. Shrotriya, J. Ouyang, R. J. Tseng, G. Li and Y. Yang, *Chem. Phys. Lett.*, 2005, **411**, 138–143.
20 F. L. Zhang, E. Perzon, X. J. Wang, W. Mammo, M. R. Andersson and O. Inganas, *Adv. Funct. Mater.*, 2005, **15**, 745–750.
21 D. Muhlbacher, M. Scharber, M. Morana, Z. G. Zhu, D. Waller, R. Gaudiana and C. Brabec, *Adv. Mater.*, 2006, **18**, 2884–2889.
22 M. Jorgensen, K. Norrman and F. C. Krebs, *Sol. Energy Mater. Sol. Cells*, 2008, **92**, 686–714.
23 K. W. Wong, H. L. Yip, Y. Luo, K. Y. Wong, W. M. Lau, K. H. Low, H. F. Chow, Z. Q. Gao, W. L. Yeung and C. C. Chang, *Appl. Phys. Lett.*, 2002, **80**, 2788–2790.
24 L. M. Chen, Z. R. Hong, G. Li and Y. Yang, *Adv. Mater.*, 2009, **21**, 1434–1449.
25 S. K. Hau, H. L. Yip, H. Ma and A. K. Y. Jen, *Appl. Phys. Lett.*, 2008, **93**, 3.
26 K. Sivula, Z. T. Ball, N. Watanabe and J. M. J. Frechet, *Adv. Mater.*, 2006, **18**, 206–210.
27 Y. Kim, S. A. Choulis, J. Nelson, D. D. C. Bradley, S. Cook and J. R. Durrant, *Appl. Phys. Lett.*, 2005, **86**, 063502.
28 X. N. Yang, J. Loos, S. C. Veenstra, W. J. H. Verhees, M. M. Wienk, J. M. Kroon, M. A. J. Michels and R. A. J. Janssen, *Nano Lett.*, 2005, **5**, 579–583.
29 X. N. Yang, J. K. J. van Duren, R. A. J. Janssen, M. A. J. Michels and J. Loos, *Macromolecules*, 2004, **37**, 2151–2158.
30 B. J. Kim, Y. Miyamoto, B. W. Ma and J. M. J. Frechet, *Adv. Funct. Mater.*, 2009, **19**, 2273–2281.
31 Y. J. Cheng, C. H. Hsieh, Y. J. He, C. S. Hsu and Y. F. Li, *J. Am. Chem. Soc.*, 2010, **132**, 17381–17383.
32 Y. J. Cheng, C. H. Hsieh, P. J. Li and C. S. Hsu, *Adv. Funct. Mater.*, 2011, **21**, 1723–1732.
33 C. H. Hsieh, Y. J. Cheng, P. J. Li, C. H. Chen, M. Dubosc, R. M. Liang and C. S. Hsu, *J. Am. Chem. Soc.*, 2010, **132**, 4887–4893.
34 C. W. Tang and S. A. Vanslyke, *Appl. Phys. Lett.*, 1987, **51**, 913–915.
35 G. Yu, J. Gao, J. C. Hummelen, F. Wudl and A. J. Heeger, *Science*, 1995, **270**, 1789–1791.
36 J. E. Slota, X. M. He and W. T. S. Huck, *Nano Today*, 2010, **5**, 231–242.
37 K. H. Lee, P. E. Schwenn, A. R. G. Smith, H. Cavaye, P. E. Shaw, M. James, K. B. Krueger, I. R. Gentle, P. Meredith and P. L. Burn, *Adv. Mater.*, 2011, **23**, 766–770.
38 C. Winder and N. S. Sariciftci, *J. Mater. Chem.*, 2004, **14**, 1077–1086.
39 K. M. Coakley, Y. X. Liu, C. Goh and M. D. McGehee, *MRS Bull.*, 2005, **30**, 37–40.
40 K. M. Coakley, B. S. Srinivasan, J. M. Ziebarth, C. Goh, Y. X. Liu and M. D. McGehee, *Adv. Funct. Mater.*, 2005, **15**, 1927–1932.
41 H. Spanggaard and F. C. Krebs, *Sol. Energy Mater. Sol. Cells*, 2004, **83**, 125–146.
42 F. S. Kim, G. Q. Ren and S. A. Jenekhe, *Chem. Mater.*, 2011, **23**, 682–732.
43 C. Y. Kuo, W. C. Tang, C. Gau, T. F. Guo and D. Z. Jeng, *Appl. Phys. Lett.*, 2008, **93**, 3.
44 J. Boucle, S. Chyla, M. S. P. Shaffer, J. R. Durrant, D. D. C. Bradley and J. Nelson, *C. R. Phys.*, 2008, **9**, 110–118.
45 A. M. Peiro, P. Ravirajan, K. Govender, D. S. Boyle, P. O'Brien, D. D. C. Bradley, J. Nelson and J. R. Durrant, *J. Mater. Chem.*, 2006, **16**, 2088–2096.
46 T. W. Zeng, I. S. Liu, F. C. Hsu, K. T. Huang, H. C. Liao and W. F. Su, *Opt. Express*, 2010, **18**, A357–A365.
47 H. Xin, F. S. Kim and S. A. Jenekhe, *J. Am. Chem. Soc.*, 2008, **130**, 5424–5424.
48 H. Xin, G. Q. Ren, F. S. Kim and S. A. Jenekhe, *Chem. Mater.*, 2008, **20**, 6199–6207.
49 B. Q. Sun and N. C. Greenham, *Phys. Chem. Chem. Phys.*, 2006, **8**, 3557–3560.
50 K. J. Ihn, J. Moulton and P. Smith, *J. Polym. Sci., Part B: Polym. Phys.*, 1993, **31**, 735–742.
51 W. D. Oosterbaan, V. Vrindts, S. Berson, S. Guillerez, O. Douheret, B. Ruttens, J. D'Haen, P. Adriaensens, J. Manca, L. Lutsen and D. Vanderzande, *J. Mater. Chem.*, 2009, **19**, 5424–5435.
52 K. Vandewal, W. D. Oosterbaan, S. Bertho, V. Vrindts, A. Gadisa, L. Lutsen, D. Vanderzande and J. V. Manca, *Appl. Phys. Lett.*, 2009, **95**, 123303.
53 S. Berson, R. De Bettignies, S. Bailly and S. Guillerez, *Adv. Funct. Mater.*, 2007, **17**, 1377–1384.
54 S. Bertho, W. D. Oosterbaan, V. Vrindts, J. D'Haen, T. J. Cleij, L. Lutsen, J. Manca and D. Vanderzande, *Org. Electron.*, 2009, **10**, 1248–1251.
55 J. S. Kim, J. H. Lee, J. H. Park, C. Shim, M. Sim and K. Cho, *Adv. Funct. Mater.*, 2011, **21**, 480–486.
56 T. Salim, S. Y. Sun, L. H. Wong, L. F. Xi, Y. L. Foo and Y. M. Lam, *J. Phys. Chem. C*, 2010, **114**, 9459–9468.
57 T. G. Jiu, P. Reiss, S. Guillerez, R. de Bettignies, S. Bailly and F. Chandezon, *IEEE J. Sel. Top. Quantum Electron.*, 2010, **16**, 1619–1626.
58 H. Xin, O. G. Reid, G. Q. Ren, F. S. Kim, D. S. Ginger and S. A. Jenekhe, *ACS Nano*, 2010, **4**, 1861–1872.
59 P. T. Wu, H. Xin, F. S. Kim, G. Q. Ren and S. A. Jenekhe, *Macromolecules*, 2009, **42**, 8817–8826.
60 G. Q. Ren, P. T. Wu and S. A. Jenekhe, *ACS Nano*, 2011, **5**, 376–384.
61 N. Kiriy, E. Jahne, H. J. Adler, M. Schneider, A. Kiriy, G. Gorodyska, S. Minko, D. Jehnichen, P. Simon, A. A. Fokin and M. Stamm, *Nano Lett.*, 2003, **3**, 707–712.
62 A. J. Moule and K. Meerholz, *Adv. Mater.*, 2008, **20**, 240–245.
63 L. G. Li, G. H. Lu and X. N. Yang, *J. Mater. Chem.*, 2008, **18**, 1984–1990.
64 Y. Zhao, S. Y. Shao, Z. Y. Xie, Y. H. Geng and L. X. Wang, *J. Phys. Chem. C*, 2009, **113**, 17235–17239.
65 J. H. Kim, J. H. Park, J. H. Lee, J. S. Kim, M. Sim, C. Shim and K. Cho, *J. Mater. Chem.*, 2010, **20**, 7398–7405.
66 S. Y. Sun, T. Salim, L. H. Wong, Y. L. Foo, F. Boey and Y. M. Lam, *J. Mater. Chem.*, 2011, **21**, 377–386.
67 B. G. Kim, M. S. Kim and J. Kim, *ACS Nano*, 2010, **4**, 2160–2166.
68 N. Kurokawa, H. Yoshikawa, N. Hirota, K. Hyodo and H. Masuhara, *ChemPhysChem*, 2004, **5**, 1609–1615.
69 C. Szymanski, C. F. Wu, J. Hooper, M. A. Salazar, A. Perdomo, A. Dukes and J. McNeill, *J. Phys. Chem. B*, 2005, **109**, 8543–8546.
70 C. F. Wu, C. Szymanski and J. McNeill, *Langmuir*, 2006, **22**, 2956–2960.
71 H. Kasai, H. S. Nalwa, H. Oikawa, S. Okada, H. Matsuda, N. Minami, A. Kakuta, K. Ono, A. Mukoh and H. Nakanishi, *Jpn. J. Appl. Phys.*, 1992, **31**, L1132–L1134.
72 H. Yabu, T. Higuchi and M. Shimomura, *Adv. Mater.*, 2005, **17**, 2062–2065.
73 K. Landfester, R. Montenegro, U. Scherf, R. Guntner, U. Asawapirom, S. Patil, D. Neher and T. Kietzke, *Adv. Mater.*, 2002, **14**, 651–655.
74 T. Piok, S. Gamerith, C. Gadermaier, H. Plank, F. P. Wenzl, S. Patil, R. Montenegro, T. Kietzke, D. Neher, U. Scherf, K. Landfester and E. J. W. List, *Adv. Mater.*, 2003, **15**, 800–804.
75 T. Kietzke, B. Stiller, K. Landfester, R. Montenegro and D. Neher, *Synth. Met.*, 2005, **152**, 101–104.
76 T. Kietzke, D. Neher, K. Landfester, R. Montenegro, R. Guntner and U. Scherf, *Nat. Mater.*, 2003, **2**, 408–412.
77 T. Kietzke, D. Neher, M. Kumke, R. Montenegro, K. Landfester and U. Scherf, *Macromolecules*, 2004, **37**, 4882–4890.
78 H. J. Snaith and R. H. Friend, *Synth. Met.*, 2004, **147**, 105–109.
79 K. Tada and M. Onoda, *Thin Solid Films*, 2005, **477**, 187–192.
80 F. S. Bates and G. H. Fredrickson, *Annu. Rev. Phys. Chem.*, 1990, **41**, 525–557.
81 C. Park, J. Yoon and E. L. Thomas, *Polymer*, 2003, **44**, 6725–6760.
82 T. L. Morkved, M. Lu, A. M. Urbas, E. E. Ehrichs, H. M. Jaeger, P. Mansky and T. P. Russell, *Science*, 1996, **273**, 931–933.
83 T. Thurn-Albrecht, J. Schotter, C. A. Kastle, N. Emley, T. Shibauchi, L. Krusin-Elbaum, K. Guarini, C. T. Black, M. T. Tuominen and T. P. Russell, *Science*, 2000, **290**, 2126–2129.
84 G. Kim and M. Libera, *Macromolecules*, 1998, **31**, 2569–2577.
85 S. B. Darling, *Energy Environ. Sci.*, 2009, **2**, 1266–1273.
86 S. M. Lindner, S. Huttner, A. Chiche, M. Thelakkat and G. Krausch, *Angew. Chem., Int. Ed.*, 2006, **45**, 3364–3368.
87 M. Sommer, S. M. Lindner and M. Thelakkat, *Adv. Funct. Mater.*, 2007, **17**, 1493–1500.

88 Q. L. Zhang, A. Cirpan, T. P. Russell and T. Emrick, *Macromolecules*, 2009, **42**, 1079–1082.
89 J. U. Lee, A. Cirpan, T. Emrick, T. P. Russell and W. H. Jo, *J. Mater. Chem.*, 2009, **19**, 1483–1489.
90 Y. F. Tao, B. McCulloch, S. Kim and R. A. Segalman, *Soft Matter*, 2009, **5**, 4219–4230.
91 M. F. Zhang, L. Yang, S. Yurt, M. J. Misner, J. T. Chen, E. B. Coughlin, D. Venkataraman and T. P. Russell, *Adv. Mater.*, 2007, **19**, 1571–1576.
92 B. W. Boudouris, C. D. Frisbie and M. A. Hillmyer, *Macromolecules*, 2008, **41**, 67–75.
93 M. C. Iovu, E. E. Sheina, R. R. Gil and R. D. McCullough, *Macromolecules*, 2005, **38**, 8649–8656.
94 M. Jeffries-El, G. Sauve and R. D. McCullough, *Macromolecules*, 2005, **38**, 10346–10352.
95 M. C. Iovu, M. Jeffries-El, E. E. Sheina, J. R. Cooper and R. D. McCullough, *Polymer*, 2005, **46**, 8582–8586.
96 C. A. Dai, W. C. Yen, Y. H. Lee, C. C. Ho and W. F. Su, *J. Am. Chem. Soc.*, 2007, **129**, 11036–11038.
97 I. Botiz and S. B. Darling, *Macromolecules*, 2009, **42**, 8211–8217.
98 I. Botiz, A. B. F. Martinson and S. B. Darling, *Langmuir*, 2010, **26**, 8756–8761.
99 J. I. Lee, S. H. Cho, S. M. Park, J. K. Kim, J. W. Yu, Y. C. Kim and T. P. Russell, *Nano Lett.*, 2008, **8**, 2315–2320.
100 C. Yang, J. K. Lee, A. J. Heeger and F. Wudl, *J. Mater. Chem.*, 2009, **19**, 5416–5423.
101 P. Peumans and S. R. Forrest, *Appl. Phys. Lett.*, 2001, **79**, 126–128.
102 H. Benten, M. Ogawa, H. Ohkita and S. Ito, *Adv. Funct. Mater.*, 2008, **18**, 1563–1572.
103 E. W. L. Chan, D. C. Lee, M. K. Ng, G. H. Wu, K. Y. C. Lee and L. P. Yu, *J. Am. Chem. Soc.*, 2002, **124**, 12238–12243.
104 Z. Liang, O. M. Cabarcos, D. L. Allara and Q. Wang, *Adv. Mater.*, 2004, **16**, 823–827.
105 Z. Q. Liang and Q. Wang, *Langmuir*, 2004, **20**, 9600–9606.
106 Z. Q. Liang, K. L. Dzienis, J. Xu and Q. Wang, *Adv. Funct. Mater.*, 2006, **16**, 542–548.
107 R. Kniprath, J. T. McLeskey, J. P. Rabe and S. Kirstein, *J. Appl. Phys.*, 2009, **105**, 124313.
108 B. Vercelli, G. Zotti, A. Berlin and M. Natali, *Chem. Mater.*, 2010, **22**, 2001–2009.
109 D. Cheyns, K. Vasseur, C. Rolin, J. Genoe, J. Poortmans and P. Heremans, *Nanotechnology*, 2008, **19**, 424016.
110 M. S. Kim, J. S. Kim, J. C. Cho, M. Shtein, L. J. Guo and J. Kim, *Appl. Phys. Lett.*, 2007, **90**, 123113.
111 M. Aryal, F. Buyukserin, K. Mielczarek, X. M. Zhao, J. M. Gao, A. Zakhidov and W. C. Hu, *J. Vac. Sci. Technol., B: Microelectron. Nanometer Struct.–Process., Meas., Phenom.*, 2008, **26**, 2562–2566.
112 X. M. He, F. Gao, G. L. Tu, D. G. Hasko, S. Huttner, N. C. Greenham, U. Steiner, R. H. Friend and W. T. S. Huck, *Adv. Funct. Mater.*, 2011, **21**, 139–146.
113 M. Aryal, K. Trivedi and W. C. Hu, *ACS Nano*, 2009, **3**, 3085–3090.
114 M. Zhou, M. Aryal, K. Mielczarek, A. Zakhidov and W. Hu, *J. Vac. Sci. Technol., B: Microelectron. Nanometer Struct.–Process., Meas., Phenom.*, 2010, **28**, C6M63–C6M67.
115 Y. Yang, M. Aryal, K. Mielczarek, W. Hu and A. Zakhidov, *J. Vac. Sci. Technol., B: Microelectron. Nanometer Struct.–Process., Meas., Phenom.*, 2010, **28**, C6M104–C6M107.
116 W. Wiedemann, L. Sims, A. Abdellah, A. Exner, R. Meier, K. P. Musselman, J. L. MacManus-Driscoll, P. Muller-Buschbaum, G. Scarpa, P. Lugli and L. Schmidt-Mende, *Appl. Phys. Lett.*, 2010, **96**, 263109.
117 S. I. Na, K. Seok-Soon, S. S. Kwon, J. Jang, K. Juhwan, T. Lee and K. Dong-Yu, *Appl. Phys. Lett.*, 2007, **91**, 173509.
118 C. F. Shih, K. T. Hung, J. W. Wu, C. Y. Hsiao and W. M. Li, *Appl. Phys. Lett.*, 2009, **94**, 143505.
119 X. M. He, F. Gao, G. L. Tu, D. Hasko, S. Huttner, U. Steiner, N. C. Greenham, R. H. Friend and W. T. S. Huck, *Nano Lett.*, 2010, **10**, 1302–1307.
120 W. J. Zeng, K. S. L. Chong, H. Y. Low, E. L. Williams, T. L. Tam and A. Sellinger, *Thin Solid Films*, 2009, **517**, 6833–6836.
121 M. Steinhart, J. H. Wendorff, A. Greiner, R. B. Wehrspohn, K. Nielsch, J. Schilling, J. Choi and U. Gosele, *Science*, 2002, **296**, 1997–1997.
122 M. Steinhart, R. B. Wehrspohn, U. Gosele and J. H. Wendorff, *Angew. Chem., Int. Ed.*, 2004, **43**, 1334–1344.
123 M. F. Zhang, P. Dobriyal, J. T. Chen, T. P. Russell, J. Olmo and A. Merry, *Nano Lett.*, 2006, **6**, 1075–1079.
124 J. T. Chen, M. F. Zhang and T. P. Russell, *Nano Lett.*, 2007, **7**, 183–187.
125 C. R. Martin, *Science*, 1994, **266**, 1961–1966.
126 J. T. Chen, D. Chen and T. P. Russell, *Langmuir*, 2009, **25**, 4331–4335.
127 D. Chen, J. T. Chen, E. Glogowski, T. Emrick and T. P. Russell, *Macromol. Rapid Commun.*, 2009, **30**, 377–383.
128 J. T. Chen, K. Shin, J. M. Leiston-Belanger, M. F. Zhang and T. P. Russell, *Adv. Funct. Mater.*, 2006, **16**, 1476–1480.
129 A. Huczko, *Appl. Phys. A: Mater. Sci. Process.*, 2000, **70**, 365–376.
130 P. Apel, *Radiat. Meas.*, 2001, **34**, 559–566.
131 D. Routkevitch, T. Bigioni, M. Moskovits and J. M. Xu, *J. Phys. Chem.*, 1996, **100**, 14037–14047.
132 D. Almawlawi, N. Coombs and M. Moskovits, *J. Appl. Phys.*, 1991, **70**, 4421–4425.
133 H. Masuda and K. Fukuda, *Science*, 1995, **268**, 1466–1468.
134 A. P. Li, F. Muller, A. Birner, K. Nielsch and U. Gosele, *J. Appl. Phys.*, 1998, **84**, 6023–6026.
135 N. Haberkorn, S. A. L. Weber, R. Berger and P. Theato, *ACS Appl. Mater. Interfaces*, 2010, **2**, 1573–1580.
136 M. K. Choi, H. Yoon, K. Lee and K. Shin, *Langmuir*, 2011, **27**, 2132–2137.
137 N. Haberkorn, J. S. Gutmann and P. Theato, *ACS Nano*, 2009, **3**, 1415–1422.
138 J. Cao, J. Z. Sun, G. Q. Shi, H. Z. Chen, Q. L. Zhang, D. J. Wang and M. Wang, *Mater. Chem. Phys.*, 2003, **82**, 44–48.
139 D. Huesmann, P. M. DiCarmine and D. S. Seferos, *J. Mater. Chem.*, 2011, **21**, 408–413.
140 H. S. Wang, L. H. Lin, S. Y. Chen, Y. L. Wang and K. H. Wei, *Nanotechnology*, 2009, **20**, 075201.
141 H. S. Wang, S. Y. Chen, M. H. Su, Y. L. Wang and K. H. Wei, *Nanotechnology*, 2010, **21**, 145203.
142 J. S. Kim, Y. Park, D. Y. Lee, J. H. Lee, J. H. Park, J. K. Kim and K. Cho, *Adv. Funct. Mater.*, 2010, **20**, 540–545.
143 J. H. Jeon, J. H. Keum, J. H. Song and J. S. Kim, *Sol. Energy Mater. Sol. Cells*, 2007, **91**, 645–651.
144 A. F. Nogueira, C. Longo and M. A. De Paoli, *Coord. Chem. Rev.*, 2004, **248**, 1455–1468.
145 P. C. Yu, C. H. Chang, M. S. Su, M. H. Hsu and K. H. Wei, *Appl. Phys. Lett.*, 2010, **96**, 153307.
146 M. H. Hsu, P. C. Yu, J. H. Huang, C. H. Chang, C. W. Wu, Y. C. Cheng and C. W. Chu, *Appl. Phys. Lett.*, 2011, **98**, 073308.
147 D. A. Rider, R. T. Tucker, B. J. Worfolk, K. M. Krause, A. Lalany, M. J. Brett, J. M. Buriak and K. D. Harris, *Nanotechnology*, 2011, **22**, 085706.
148 M. K. Fung, Y. C. Sun, A. Ng, A. M. C. Ng, A. B. Djurisic, H. T. Chan and W. K. Chan, *ACS Appl. Mater. Interfaces*, 2011, **3**, 522–527.
149 K. M. Coakley, Y. X. Liu, M. D. McGehee, K. L. Frindell and G. D. Stucky, *Adv. Funct. Mater.*, 2003, **13**, 301–306.
150 K. M. Coakley and M. D. McGehee, *Appl. Phys. Lett.*, 2003, **83**, 3380–3382.
151 H. Wang, C. C. Oey, A. B. Djurisic, M. H. Xie, Y. H. Leung, K. K. Y. Man, W. K. Chan, A. Pandey, J. M. Nunzi and P. C. Chui, *Appl. Phys. Lett.*, 2005, **87**, 023507.
152 C. C. Oey, A. B. Djurisic, H. Wang, K. K. Y. Man, W. K. Chan, M. H. Xie, Y. H. Leung, A. Pandey, J. M. Nunzi and P. C. Chui, *Nanotechnology*, 2006, **17**, 706–713.
153 S. S. Kim, J. Jo, C. Chun, J. C. Hong and D. Y. Kim, *J. Photochem. Photobiol., A*, 2007, **188**, 364–370.
154 H. J. Her, J. M. Kim, C. J. Kang and Y. S. Kim, *J. Phys. Chem. Solids*, 2008, **69**, 1301–1304.

